UNIVERSITY OF OKLAHOMA

GRADUATE COLLEGE

A GRAVITY AND MAGNETIC STUDY OF THE STRUCTURE EVOLUTION OF SICHUAN BASIN

A THESIS

SUBMITTED TO THE GRADUATE FACULTY

in partial fulfillment of the requirements for the

Degree of

MASTER OF SCIENCE

By

LI PAN
Norman, Oklahoma
2016

A GRAVITY AND MAGNETIC STUDY OF THE STRUCTURE EVOLUTION OF SICHUAN BASIN

A THESIS APPROVED FOR THE
CONOCOPHILLIPS SCHOOL OF GEOLOGY AND GEOPHYSICS

BY

_____
Dr. Michael J. Soreghan, Chair

_____
Dr. G. Randy Keller

_____
Dr. John D. Pigott

Acknowledgements

This thesis work was carried out during the cold winter of oil price in declines in 2015. It would have never been completed without the support and assistance of many dedicated individuals.

First of all, I would like to express my great gratitude to my academic advisor Dr. G. Randy Keller. He has not only given me instructive advice during the process of the work, but also has consistently encouraged me when I was in difficulties. Without his patience and supervision, I would not be able to finish this thesis. I am particularly grateful to Dr. Michael J. Soreghan and Dr. John D. Pigott for their insightful suggestions in revising my thesis.

I would like to extend my truehearted thanks to Dr. Xinguo Duan, Professor from Chengdu University of Technology, for his generous assistance in providing 2-D seismic data and formation tops in my study area. Also, Dr. Hongyan Shen, Professor from Xi'an Shiyou University, has provided important advice for my gravity and magnetic data analysis.

Besides, I sincerely appreciate that Mr. Richard D. Andrews from Oklahoma Geological Survey and Mr. David M. Thomas III from Trey Resources Inc. for providing me research assistant and intern positions. Thanks to their support, I can have free access to key software packages (Oasis Montaj software at the OGS and GeoGraphix at Trey Resources). I would like to thank all my classmates and friends in ConocoPhillips School of Geology and Geophysics. They all cheered me up in the oil market downturn and kept me striving to develop as a geologist.

Finally, I wish to thank my family for their support and encouragement throughout my study. My appreciation goes beyond language.

Table of Contents

List of Tables

List of Figures

Abstract

The Sichuan Basin and its adjacent area have attracted increasing research attention during the past decade. Although damaging earthquakes occurred in 2008, the natural gas potential in this region is also remarkable. Therefore, it is important to carry out detailed research on the structure evolution of the Sichuan Basin and how it relates to local hydrocarbon accumulations and possibly earthquake hazards. Previous studies on the tectonic evolution of the region have revealed a complex structure beneath the periphery of Sichuan Basin. In this study, the modern gravity and magnetic data were employed and analyzed, which contributed to the deep tectonic structural interpretation. A significant NW to SE oriented gravity anomaly increase indicates that the crustal thickness decreases from Songpan - Ganzi terrane into the Sichuan Basin. A strong horizontal gravity gradient belt clearly follows the Longmenshan fault-thrust belt. The central paleo-uplift in the Sichuan Basin correlates with high gravity and magnetic anomaly values. The western boundary of the Sichuan Basin exhibits several scattered positive magnetic anomalies, which correlate with Precambrian igneous intrusions. Based on the data from China National Petroleum Company, three seismic reflection profiles were utilized to study the sedimentary characteristics and shallow structural deformation in the Sichuan Basin. According to these seismic profiles, the Longmenshan orogeny and western Sichuan foreland basin subsidence provided the matter-source and accommodation space for the deposition of the Xujiahe Formation in the Late Triassic. Across the area with the best data coverage, an integrated 2-D geologic model is generated by all geological and geophysical controls. The inversion model clearly displays the geometry of crustal structure variations and shallow strata

deformations. The central paleo-uplift stands out as gravity high along the model profile. The Northwestern Depression and Southeastern Depression have gentle sedimentary thickness variations, and both attenuate upward toward the paleo-uplift. The Longmenshan fault-thrust belt represents the most complex crustal structure in the area with older formations superposed on younger formations. Large faults are well developed, which make it an earthquake-prone region as well as, a significant unconventional gas reservoir.

Keywords*: Foreland basin, Longmenshan, paleo-uplift, gravity anomaly, magnetic anomaly, seismic profiles, 2-D integrated model*

Chapter 1. Introduction

The Sichuan Basin with an area of about 230,000 km^2, is located in southwest China, and is one of the earliest areas of natural gas drilling and utilization in the world (Jiang et al., 2001). According to Chinese history records, around 76-147 AD the indigenous people in the western Sichuan Basin started to dig wells to get brine, and used the associated natural gas to evaporate the water and recover the salts. Late in 1041 AD, cable-tool drilling was invented and a unique well-drilling system was developed to extract and utilize natural gas (Li, 2011). Compared with coal combustion, natural gas has less CO_2 emission and pollutants and is widely endorsed as clean energy. As a consequence of environmental stresses, the natural gas industry has been promoted as a national energy strategy in China. Therefore, the Sichuan Basin has become a revitalized optimal basin for shale and tight sand gas exploration by Chinese national oil companies with government policy leverage. Today, the central and west Sichuan Basin are targeted areas for conventional and unconventional exploration. Restricted data from China National Petroleum Company (CNPC), the largest owner of Sichuan gas fields, has shown that there are 113 gas fields have been discovered, with 1371 billion m^3 of proved reserves and 813 billion m^3 of recoverable reserves. In 2009, the Sichuan Basin produced over 15 billion m^3 of natural gas (Li, 2011).

Another feature that made Sichuan Basin well known is its frequent occurring geologic hazards. The mountainous and plateau areas surrounding Sichuan Basin, suffer active landslides, mud-rock flows and cliff collapses due to the complicated geological conditions. Furthermore, the destructive and unpredictable earthquakes are threatening the safety of local residents. According to China Earthquake Networks Center, the

Wenchuan Earthquake (Ms 8.0, 2008) and Ya'an Earthquake (Ms 7.0, 2013), occurred along the NE trending Longmenshan fault-thrust belt, which separates the Sichuan Basin from the Songpan-Ganzi terrane. The tremendous earthquakes claimed more than sixty thousand lives and incalculable economic loss, and millions of victims lost their homes, which are the severest earthquakes in modern China records (SPPG, 2009; DCASP, 2013). Thus, research on regional structure and tectonic movement can help to further understand local geological conditions and contribute to disaster prevention and control.

This integrated study was designed to describe and interpret the tectonic evolution of the Sichuan Basin, especially the western Sichuan foreland basin, and its implications on regional geologic hazards and hydrocarbon exploration. The dominant part of this thesis is the comprehensive geophysical data processing and integrated interpretation of the study area. The research results are presented in three steps: firstly the latest potential field data is processed and interpreted. These data were obtained from Bureau Gravimetrique International (BGI)'s World Gravity Map (WGM) 2012 project and World Digital Magnetic Anomaly Map (WDMAM)'s database. This study focused on the interpretation of deep structural framework and crystalline basement petrology. Secondly, the potential field data was integrated with seismic reflection data analysis. Three seismic reflection profiles were available to be employed in this study, and document the regional sedimentary characteristics and shallow strata deformation. Finally, a 2-D integrated geological/geophysical model was constructed using all the available data as controls.

Chapter 2. Geologic Setting

The Sichuan Basin (Figure 2.1), situated in the western Yangtze Craton and also called South China block (SCB), is a large complex, diamond shape petroliferous superimposed basin ranging from 28°N~32°40'N, 102°30'E~110°E (Wang et al., 2002). The Sichuan Basin has experienced complex tectonic movements as a foreland basin during Late Mesozoic-Cenozoic overlying a Proterozoic–Middle Mesozoic passive margin (Ma et al., 2007). Figure 2.1 shows the broad tectonic framework of the entire Sichuan Basin and its adjacent area. In Late Middle Triassic, the North China block (NCB) and South China block (SCB) along the Qinling-Dabie orogen collided and formed the Qinling thrust system, which shapes the northern edge of the Sichuan Basin (Meng and Zhang, 1999; Meng et al., 2005). The west side of the basin is the well-known Longmenshan fold-thrust belt (FTB) that extends in a NE direction at high angle to the Qinling-Dabie orogen. Since it lies between the SCB and Songpan-Ganzi Terrane (SGT), it is probably related to the amalgamation of the NCB and SCB. The north boundary of the Sichuan Basin is the Micangshan - Dabashan FTB, which displays an irregular structural shape. The Micangshan uplift trends NEE, while the Dabashan FTB is an arc-shaped nappe, trending NW-NWW (Zhang et al., 2013) (Figure 2.1). In Late Jurassic, the Dabashan FTB formed and was overlapped on earlier Triassic folds (Dong et al., 2006, 2010; Zhang et al., 2013). The Micangshan FTB was formed in the Early Cretaceous (Meng et al., 2005). These two structural belts separate the Sichuan Basin from the Qinling orogen. The southeast and the southwest portions of the basin are also widely controlled by thrust-folding system, namely the East Sichuan FTB and the Southwest Sichuan FTB (including Xianshuihe and Shimian

Faults, Figure 2.1). These features are the result of uplifting and deformation during the Himalayan orogeny and outline the south boundary of the Sichuan Basin (Hao et al., 2008).

2.1 Stratigraphy and Basin Evolution

Figure 2.3 shows a generalized stratigraphy and tectonic history of the Sichuan Basin (modified from Wang, 1989; Ma et al., 2007). The crystalline basement of the Yangtze craton formed about 1700 Ma, during Zhongtiao orogeny of Pre-Sinian age (Huang et al., 2009). These deposits are mainly composed of high-grade metamorphic and igneous rocks and low-grade metasedimentary rocks (Jia et al., 2006). At about 850 Ma, a suite of folded basement rocks was emplaced during Jinning and Chengjiang age deformation to overlie the crystalline rocks (Sichuan Bureau of Geology and Mineral Resources, 1991; Huang et al., 2009). During the Jinning period, the Yangtze craton witnessed significant rifting, with deposition of ~ 1000m thick volcanic deposits (Huang et al., 1987; He et al., 2011). Based on previous gravity, magnetic, seismic, and well-logging data, the basement formed during the Jinning tectonism and can be separated into the Northwestern Depression, Central paleo-uplift, and Southeastern Depression (Figure 2.2). The depression's basement consists of weakly magnetic, metamorphic rocks, with a depth of ~8-11 km. In contrast, the uplifted basement consists of strongly magnetic acidic volcanic rocks and metamorphic rocks, with a depth of ~6-8 km (Chen et al., 1994; Jiang et al., 2001; Huang et al., 2009). Where after, a long-term transgression occurred, throughout the entire Yangtze craton that lasted from the Sinian to Middle Silurian.

Structurally, the Sichuan Basin is surrounded by fold-thrust belts (Jiang et al., 2001; Meng et al., 2005; Ma et al., 2007). The Yangtze craton has mostly been characterized by subsidence (Figure 2.2). The basin can be divided into three main subdivisions, the NW Depression, the Central paleo-uplift, and the SE Depression, bounded by the Longquanshan fault on the west and the Huayingshan fault on the east. Studies of the basement within the basin show that six tectonic cycles can be recognized, Yangtze, Caledonian, Hercynian, Indosinian, Yanshanian and Himalayan (Wang, 1989; Ma et al., 2007) (Figure 3). The Central paleo-uplift was developed in two stages, the Leshan-Longnvsi paleo-uplift (Longnvsi located in Wusheng) was formed during the Caledonian orogeny and the Luzhou-Kaijiang paleo-uplift was formed during the Indosinian orogeny (Figure 2.2). In general, the evolutionary process of the Sichuan Basin can be divided into three phases, Middle Proterozoic-Early Paleozoic craton depression, Late Paleozoic-Early Middle Triassic intracratonic rift depression, and Late Triassic-Middle Cenozoic foreland basin stage (He et al., 2011).

During the Middle Proterozoic-Early Paleozoic craton depression stage, the Sichuan Basin area was a stable part of the Yangtze craton. Intraplate uplift and basin margin uplift developed the rudiment of the Sichuan Basin as bounded by the Leshan-Longnvsi uplift and the Longmenshan marginal uplift. These uplifts were significantly different; the marginal uplift is associated with the later orogeny while the intraplate uplifts set the foundation for sedimentation of the basin strata.

The second phase of the development were the Late Paleozoic-Early Middle Triassic intracratonic rift depression stage. The opening of the Paleo-Tethys Ocean developed the south, west and north portion of the SCB as passive continental margins,

which gave rise to the extensional structure of upper Yangtze and peripheral area during the Hercynian. In the Permian, the extension was accelerated (Emei taphrogeny; Luo et al., 2004; Jia et al., 2006). The eruption of basalt marked the peak of extensional movement in the Late Permian. This “Emei mantle plume” theory might explain the kinetic mechanism of the Yangtze craton’s eastward migration during the Late Permian and Early Triassic (Luo, 1991; Luo et al., 1992). The Indosinian movement in the Late Middle Triassic ended the craton marine basin sedimentation. The Upper Triassic sedimentation started in the Indosinian.

Relating to the closing of Paleo-Tethys Ocean, during the Late Triassic-Middle Cenozoic foreland basin stage, the Songpan-Ganzi terrane was gradually uplifted and folded intensely and thrusted eastward and formed the Longmenshan thrust-nappe structure (Liu et al., 1995). The sedimentary area extended to the east and connected with the western Sichuan foreland basin. By the end of the Late Triassic, the foreland basin transformed into a terrestrial lacustrine basin.

2.2 Lithology of Major Stratigraphic Units

During the Late Sinian, Doushantuo Formation (Z_1) formed as a dolomite interbedded with black shale, unconformable overlapping on Pre-Sinian strata. The Dengying Formation (Z_2, Figure 2.3) is a ~600-1200 m thick dolomite interbedded with shale (He et al., 2011). Rocks of Cambrian age are dominated by shale and carbonates. In particular, the Lower Cambrian Qiongzhusi Formation ($\in_1$) is one of the main shale targets (Li, 2011). Ordovician rocks were deposited in shallow-marine and non-marine environments, with a stable thickness of ~ 400-600 m (He et al., 2011). Silurian strata are thicker from west to the east, ranging from 100-1200 m, with the depocenter in the

SE Depression. Deposits of the Devonian and Carboniferous are absent throughout almost the entire western Sichuan Basin subsurface. However, thick strata of these ages are found within the Longmenshan FTB, where the thickness can reach ~2000-4000 m (Burchfiel et al., 1995; Chen et al., 2005; Jia, et al., 2006). It suggests the Leshan-Longnvsi paleo-uplift during the Caledonian orogeny and the extensional process during the Silurian-Carboniferous occurred along the western margin of the South China block (Chen and Wilson, 1996; Chen et al., 2005).

The Caledonian orogeny in the Late Silurian established the framework of the NE-trending Central paleo-uplift and interrupted the marine deposition (Ma et al., 2007). During this time, the entire basin experienced severe uplift, denudation, folding, and magmatic intrusion. As a result, the SE Depression, situated in the eastern slope of the Central paleo-uplift, contains mainly Devonian strata, and Carboniferous deposition was limited to the eastern part of the Sichuan Basin (Cai et al., 2003).

The second major transgression happened at the end of Carboniferous, when ~ 400-900 m of Permian strata accumulated, which was dominated by shallow water limestone and dolomite (Jia et al., 2006). The Middle Permian experienced a major eruption of basalt (Luo et al., 2004; Jia et al., 2006). Early Triassic inherited the Late Permian tectonic sedimentary setting. Carbonate slope to carbonate platform deposits, named Feixianguan Formation (T_1f) (~300-550m thick) and Jialingjiang Formation (T_1j) (~400-600m thick) formed on the Upper Yangtze craton (He et al., 2011). The Feixianguan Formation is the major gas bearing layer of northeastern Sichuan Basin. Sea level changed significantly in Middle Triassic, which led to the deposition of Leikoupo Formation (T_2l) with ~200-900 m in thickness (He et al., 2011). Late Triassic

is the key period for the transition of Sichuan Basin when the Paleo-Tethys Ocean closed. The South China block experienced a regression and developed into a foreland basin with paleo high in the east and low in the west. Luzhou-Kaijiang paleo-uplift started, as an outcome of Indosinian orogeny. Figure 2.4 is an isopach map of the Upper Triassic, showing the ~250-4000 m thick Xujiahe Formation, with visible thinning in the SE and the thickening in the NW.

The Lower and Middle Jurassic strata lay unconformably on the Upper Triassic strata along the southeast slope of Longmenshan FTB. Upper Jurassic and Lower Cretaceous strata increased in thickness toward to north in the NW Depression, suggesting the foredeep subsidence of this period along the Micangshan (Jia et al., 2006). The Cenozoic sediments merely occurred in the southern part of the basin and along the foothills of the Longmenshan. Overlain on these areas, Paleogene strata deposited conformably and formed the fluvial-lacustrine red beds (Jiang et al., 2001, Jia, et al., 2006).

2.3 Historical Earthquake Analysis - Case study of Wenchuan Earthquake

Figure 2.5 and Figure 2.6 separately show locations of epicenters of earthquakes greater than Ms 6.0 and Ms 3.0 from 1900 to 2016, according to China Earthquake Network Center (CENC), from which the frequent earthquake activities of Longmenshan is apparent. In Figure 2.5, the Wenchuan and Ya'an are marked as blue and magenta arrow respectively. Comparing these two figures, the epicenters of Ms 6.0 and above are all distributed along the Longmenshan FTB. While inside the basin fewer earthquakes occurred, which suggests the stability of the Yangtze craton beneath. The Wenchuan earthquake (Ms 8.0) event occurred northwest of Chengdu on May 12,

2008 and is the most severe earthquake taken place in China in the past century. Due to its shallow hypocenter and high magnitude, a large area suffered seismic intensity X-XI effects, the hard-hit area stretched for over 50 km^2 (Fu et al., 2008). By Aug 14, 2008, there were altogether 23,880 aftershocks in the Longmenshan and the adjacent area, of which there were 259 Ms.4.0 earthquakes, 39 Ms.5.0 ~ 5.9 earthquakes, and 8 Ms 6.0 ~ 6.4 earthquakes.

Chapter 3. Previous Geophysical Studies

As one of the major petroliferous areas in China, almost all the previous geological and geophysical studies of the Sichuan Basin were driven by hydrocarbon exploration. Released by Sichuan Bureau of Geology and Mineral Resources and China National Petroleum Corporation, the earliest scientific exploration in this basin started with drilling wells around oil seeps and 2-D seismic surveys in 1950s (Jia et al., 2006). The first commercial gas field, Zhongba gas field, was discovered by CNPC in 1971, which has an accumulated production of 1.2×10^{10} m^3 (Jia et al, 2006). Since then, more than 300 wildcat wells and production wells have been completed, and the discovery of several large gas fields in the western and central Sichuan Basin has encouraged more petroleum exploration and research (Jia et al., 2006; Ma et al., 2007). More recently, high-resolution 2-D and 3-D seismic surveys of the area have been carried out, and wildcat wells were drilled in the early 1990s (Ma et al., 2007). All major gas-bearing layers are presented in Figure 2.3 (Dengying Formation-Sinian, Huanglong Formation-Carboniferous, Maokou and Changxing Formation-Permian, all Triassic formations, and Penglai Formation-Jurassic). Figure 3.1 shows the 125 natural gas fields in the Sichuan Basin, based on the statistics of China Ministry of Land and Resources (Ma et al., 2010). Among them, general features of the top 14 gas fields are listed in Table 3.1, showing that the discovered gas fields produce from multiple reservoir layers, notably in the Permian, Triassic and Jurassic.

3.1 Seismic Survey

In 1988, CNPC deployed a regional natural gas exploration project, consisting of six long 2-D seismic lines in central – northwestern Sichuan to refine the regional

subsurface geology. Out of confidentiality in business competition and other political reasons, the data of these seismic profiles were restricted from publications. Since the Wenchuan earthquake, the rising attention focused on this area resulted in the release of these confidential data. In 2011, the seismic profile along Section A (Figure 3.2) was analyzed and published in the Chinese Journal of Geology (He et al. 2011). In this study, the authors identified nine regional unconformities in the seismic data, and analyzed evolution of the Central paleo-uplift and Longmenshan orogen. This thesis includes an analysis of three seismic lines of Dr. Xinguo Duan and his team's unpublished interpretation in Chapter 4.

3.2 Gravity and Magnetic Survey

Like the seismic survey, the majority of previous gravity and magnetic surveys were served for oil and gas exploration. Before 2000, studies were carried out by local geological surveys without an integrated map for the entire Sichuan Basin. In 2001, Jiang et al. (2001) published a comprehensive study of Sichuan Basin based on merging previous gravity and magnetic surveys. They defined a high gravity gradient belt beneath the Longmenshan fault zone. A gravity anomaly high along the Central paleo-uplift was also found. In addition, Jiang et al. (2001) stressed the entire basin is surrounded by negative magnetic anomalies. They also noted that the positive magnetic anomalies inside the basin are distributed as a rough diamond shape.

After the Wenchuan earthquake, new data, particularly satellite gravity and aeromagnetic data, were available for deep structure analysis in Longmenshan range. Zhang (et al., 2009, 2010) described the relationship between the earthquakes and gravity/magnetic anomalies in Longmenshan range. They stated that the Longmenshan

gravity gradient belt belongs to the major gradient belt surrounding the Tibetan plateau (Zhang et al., 2009). Based on their analysis of the Wenchuan earthquake and aftershocks, most of earthquakes in the region occurred in the upper and middle crust. Thus, they believed that there is an interface between units with different densities beneath the Longmenshan range. They concluded that the movement of the brittle continental block along this density interface is a likely location for earthquakes.

Chapter 4. Geophysical Analysis

This chapter is composed of an analysis of gravity, magnetic, seismic reflection, and geologic data followed by construction of an integrated 2-D model across key areas in the basin. Gravity and magnetic data analysis plays an important role in conducting geophysical mapping and interpretation of lithospheric structure and geodynamic processes (Keller et al., 2002). Given the relatively easy data acquisition and open source effective software tools, gravity and magnetic methods are ideal for integrated analysis with geological data, seismic data, Digital Elevation Model (DEM) data, etc. In addition, satellite data can enhance the study of deep structure with the presentation of long wavelength gravity anomalies. A gravity survey is a precise differential measurement of the Earth's gravity field, which is straightforward to process and interpret. The variation of density in the subsurface can be inferred after basic physical laws are employed to remove predictable variations in the gravity field. In contrast, a magnetic survey is sensitive to variations in the Earth's magnetic field, which reveals differences in crustal magnetization related to geologic processes. With the joint analysis of seismic data, the spatial resolution can be improved and the integrated density model can be more accurate.

4.1 Gravity Data Analysis

4.1.1 Data and Methods

The gravity data used in this thesis was obtained from the database of WGM2012 global model (http://bgi.omp.obs-mip.fr/data-products/Grids-and-models/wgm2012) that is maintained by the BGI (Bureau Gravimetrique International). The World Gravity Map (WGM) is a set of education and research open source, high-

resolution gravity anomaly maps and digital grids computed at global scale (Bonvalot et al, 2012). In 2012, BGI released its latest version, which consists of three major anomaly maps, surface free-air, complete Bouguer and isostatic anomalies. The WGM2012 global model is the first release of a high-resolution grid (2 arc-minute resolution, ~3.7 km) of the Earth's gravity anomalies, which are derived from the available Earth global gravity models EGM2008 and DTU10 (Andersen, 2010) and include terrain corrections derived from ETOPO1 digital topographic model (Amante and Eakins, 2009) that considers the contribution of most surface masses (Bonvalot et al, 2012). Comparing to EGM2008's 2.5 arc-minute resolution, WGM2012 model improves the accuracy of gravity anomaly data, and contributes to building more precise density modeling results.

A gravity anomaly is the difference between the observed gravity value and that predicted from a theoretical Earth model. A positive anomaly suggests the location is characterized by a higher gravity value than predicted, while a negative anomaly indicates a lower value than predicted (Heiskanen and Moritz, 1967). Complete Bouguer Anomaly (CBA) is refined gravity anomaly with corrections applied to latitude, elevation, terrain, etc. The height correction alone defines a Free Air Anomaly (FAA) (Li and Götze, 2001). In this study, these two types of anomaly datasets from the WGM2012 dataset were employed and analyzed using Oasis Montaj software (www.geosoft.com/products/oasis-montaj/overview). All data were projected to the WGS 84 datum, which is a conventional terrestrial reference system. The study area is located in UTM zone 48N, restricted as 27˚ to 35˚ latitude by 102˚ to 110˚ longitude,

which covers the entire Sichuan Basin and its adjacent areas. The minimum curvature technique with 5km grid spacing was employed in gridding for map construction.

Oasis Montaj offers two color schemes for image visualization. A linear color scheme is defined as a transform method for zoning the data, which divides the range of grid values linearly into even increments. In contrast, a histogram color scheme provides a color tool that evaluates the grid values and statistically determines the zones so that each color occupies an equal area of the map.

For further analysis of the subsurface structure characteristics of the Sichuan Basin, three filters (upward continuation, residual gravity analysis, and horizontal gradient magnitude) were applied to the original Bouguer gravity anomaly data. Upward continuation acts as a low-pass filter, which attenuates surface features and noise (Blakely, 1996). In other words, upward continuation simulates the gravity values as if they were measured at a higher elevation, which smooths the anomalies and accentuates deeper features. In 2001, Jiang at al. (2001) suggested that the Moho depth underneath the Sichuan Basin ranges from 38-41 km, while the study from Zhang (2010) showed that the Moho depth varies from 42-44 km (Zhang et al., 2010). Thus, a depth of 40 km was employed to generate the upward continuation gravity grid, which displays the trends of density variation below the Moho depth. In contrast, a residual gravity map is made by using point-by-point subtraction of the upward continued grid from the original CBA grid, which acts as a high-pass filter and emphasized upper crustal anomalies. For example, a residual gravity map after 40 km upward continuation primarily represents the density variation within the crystalline crust and the overlying stratum. In an attempt to effectively recognize and emphasize the structural details of

study area, such as edges and trends of subsurface geologic bodies, a horizontal gradient magnitude (HGM) filter was applied.

4.1.2 Observations and Interpretations

Figure 4.1 and Figure 4.2 display the digital elevation (DEM) and the Free Air anomaly (FAA) maps, respectively. The DEM map illustrates that the Sichuan Basin is entirely surrounded by mountains and fold-thrust belts. The highest elevation in the study area is located in the Longmenshan and Songpan-Ganzi terrane, while the lowest elevation lies in the center of the basin (Figure 4.1). Comparing these two figures, the FAAs generally follow the topographic configuration, where high topography of Longmenshan, Qinling, Micangshan, Dabashan, Southwest Sichuan fault-thrust belt (FTB), and East Sichuan FTB all exhibit high FAA values (red or magenta areas in Figure 4.2); and low topography of the NW Depression, SE Depression, north and south Qinling intermountain basins all display low FAA values (blue areas in Figure 4.2).

The deviations between the DEM and FAA can be explained as the heterogeneity within the subsurface geology. For instance, the central basin represents moderate FAA values (yellow and light green areas in Figure 4.2) but low topography (dark blue areas in Figure 4.1), which indicates a relatively shallower basement.

The next step in my analysis was to create a grid of Complete Bouguer anomaly (CBA) values and filtered grids of it to enhance integrated gravity interpretation. The CBA values in the Sichuan Basin area were displayed in three visualizations: histogram color scheme (default in Oasis Montaj) without a color shaded relief grid, linear color scheme without a color shaded relief grid, histogram color scheme co-rendered with a color shaded relief grid, respectively in Figures 4.3, 4.4, and 4.5. Comparison of these

figures shows that the histogram map accentuates values of anomalies, while the linear method better outlines the anomaly boundaries. The co-rendered shaded relief grid provides a visual effect that is 3-D in nature. The following gravity and magnetic maps (Figure 4.6 – Figures 4.14) are all colored with the histogram scheme co-rendered with a shaded relief grid.

The Sichuan Basin is associated with a large range of Complete Bouguer anomaly values, due to major subsurface structures in and around it (Figure 4.5). Overall, the study area is entirely characterized by distinct negative gravity anomalies. Anomaly values generally become less negative from NW to SE, which suggests the crustal thickness decreases from NW to SE. The Songpan-Ganzi terrane displays in the lowest gravity values, surrounded by a significant gravity gradient belt, ranging from -240 mGal to -320 mGal, which clearly outlines the Longmenshan FTB. In addition, the Southwest Sichuan FTB also coincides with a gravity gradient belt, ranging from -120 mGal to -200 mGal. These two gradient belts converge near the city of Ya'an, the epicenter of 2013 Ya'an earthquake.

Inside the basin, especially the central paleo-uplift area, the Bouguer gravity anomalies range only from -80 mGal to -120 mGal (Figure 4.5). There is a large northeast-trending gravity maximum near the city of Chongqing (> -80 mGal). In addition, there exists a northeast-trending gravity minimum just east of the city of Nanchong (<-120 mGal). Overall, the area of the basin is a high gravity anomaly, which indicates a relatively thin crust and/or a paleo-uplift. Linear gravity gradients are also within the basin, which can be interpreted as fault zones. For example, along the northwest and southeast edges of the central paleo-uplift, there are two prominent linear

gravity gradients belts that generally follow the Longquanshan and Huayingshan fault zones (Figure 4.5). The northwest gravity gradient belt increases gravity anomaly value prominently from -200 mGal to -120 mGal, while the southeast one decreases gravity value from -100 mGal to -120 mGal (Figure 4.5). Other local anomalies could indicate local sub-basin/depressions or igneous intrusions (Figure 2.2). Overall, the gravity anomalies inside the basin rough generally fit Sichuan Basin defined geographically.

Figure 4.6 shows a 40 km upward continuation filtered CBA map, and the Longmenshan FTB is shown as an obvious green gravity gradient belt (from -250 mGal to -170 mGal), which separates Sichuan Basin and the Songpan-Ganzi terrane. Meanwhile, the SW Sichuan FTB also follows a distinct green gravity gradient belt (from -250 mGal to -180 mGal), which shaped the basin's southwest edge. These two gravity gradient belts converge on Ya'an, which might reveal the mechanism of 2013 Ya'an Earthquake.

Compared with the CBA map (Figure 4.5), the high gravity anomaly to the west of Chongqing still can be seen in the 40 km upward continued CBA map (Figure 4.6), which implies the anomaly might be a result of a deep density variation. On the other hand, the low gravity anomaly in Nanchong is not as noticeable as in Figure 4.5, indicating that the anomaly body is buried at a relatively shallow depth. Along with the Longmenshan gravity gradient belt, the Longquanshan fault belt is also clearly illustrated as the yellow belt between Chengdu and Nanchong in Figure 4.6.

Figure 4.7 shows a 100 km upward continuation filtered version of the original CBA map that simulates the measurement elevation as 100 km above the Earth's

surface. Comparing Figures 4.6 and 4.7, the regional gravity trend is almost the same, which suggests that the deep crust of the Sichuan Basin thins gradually from NW to SE.

Figures 4.8 and 4.9 are residual gravity maps, generated by subtraction of upward continued grids at 40 km and 10 km from the original CBA, respectively. Both residual maps mainly represent variations of intrabasement structure and the thickness overlying strata of the study area. The magenta-red high anomalies outline the shape of the Sichuan Basin. These maps clearly distinguish the basin from the surrounding mountains.

Comparing the two residual maps and the original CBA map, the area west of Chongqing appears as a gravity anomaly high in all three figures, which indicates the core of the central paleo-uplift, is located in this area. However, the high gravity anomalies in the Leshan area and the area to the east in the two residual maps, suggest the Leshan-Longnvsi paleo-uplift (blue circle in two residual maps) during the Caledonian orogeny (Ordovician - Early Devonian) developed the first stage of Central paleo-uplift. An interesting feature is evident when comparing the two residual maps, that is, the central basin gravity high is slightly shifted eastward from crystalline crust to shallower layers. Kaijiang, for example, in the 10 km upward residual map (Figure 4.9) shows a higher gravity anomaly than in the 40 km upward residual map (Figure 4.8). This indicates the existence of the second stage of Central paleo-uplift, Luzhou-Kaijiang paleo-uplift (yellow circle in two residual maps) during the Indosinian orogeny (Late Permian - Triassic). In other word, the Luzhou-Kaijiang paleo-uplift made a shallower crust. In addition, areas such as Wenchuan indicate that isolated bodies in the upper crust are coincident with local igneous intrusions (Figure 2.2). The local gravity

highs and lows represent local uplifts and sub-basins that generally correlate with the Sichuan oil/gas fields (Figure 3.1).

Figures 4.10 and 4.11 show the original CBA map and the 40 km upward continuation residual gravity map after application of the Horizontal gradient magnitude (HGM) filter. In both maps, the steepest gradients denote the edges of the Longmenshan FTB (high values shown in magenta). The complex shape of this belt suggests that its deep structure is complex. The strong NE-trending high gradients (0.4 – 0.5 mGal/km) in the area west of Chongqing indicate the complexity of the Central paleo-uplift (Figure 4.10).

4.2 Magnetic Data Analysis

4.2.1 Data and Methods

Measurements of anomalies in Earth's magnetic field are also a helpful and cost-efficient method to aid geological research (e.g., Keller et al., 2006). The characteristics of magnetic anomalies are a composite of regional structural deformation and magnetic body distribution. The magnetic data used in this thesis was obtained from the World Digital Magnetic Anomaly Map (WDMAM) project, which incorporates all available aeromagnetic and satellite magnetic anomaly data internationally. The WDMAM is defined as a global magnetic intensity anomalies grid (3 arc-minute resolution, ~5.5 km) at a 5 km elevation above average sea level (http://models.geomag.us/wdmam.html). It was compiled from satellite, marine, aeromagnetic and ground magnetic surveys. The long-wavelength satellite data was obtained from the CHAMP satellite for geoscientific and atmospheric research and applications (GFZ, 2016), and the short-wavelength aeromagnetic compilation of China was provided by Getech (2016).

The gravity and magnetic fields of the Earth are vector fields. The geometric vector is a mathematical quantity with both direction and magnitude (Blakely, 1996). In magnetics, the field directions vary from horizontal (magnetic equator) to vertical (magnetic poles), and remanent magnetism can often be strong related to the induced component. Thus, reduction to the pole (RTP) was employed to remove the effects of magnetic inclination. The geomagnetic inclination in the study area is 47.25°, and the declination is -2.34°.

4.2.2 Observations and Interpretations

Figure 4.12 shows the map of total magnetic intensity (TMI) obtained by RTP of the study area, which has TMI values mainly distributed from -150 nT to 200 nT. The northern Longmenshan FTB is associated with a prominent NE oriented negative anomaly, with the lowest intensity is under -150 nT. Separated by Longmenshan FTB, the west part of the study area, specifically the Songpan-Ganzi terrane, is characterized by weak negative magnetic anomalies, ranging from -75 to -30 nT. Except for some small areas, e.g. east across the Micangshan FTB (Fig. 2.1), the entire northwestern half of the Sichuan Basin contains broad positive anomalies. The maximum of the magnetic intensity is over 200 nT near Nanchong. The Leshan-Nanchong-Wanyuan high anomaly belt is associated with a strong NE-trending negative magnetic anomaly belt to its north, (Zhang et al, 2010). Frey (1982) compared satellite magnetic anomalies on a global basis with known geologic and tectonic structures, and proposed that the positive magnetic anomalies generally coincide with shields, cratons, platforms, submarine plateaus, and subduction zones. Thus, some scholars support the hypothesis that the

Sichuan Basin might have a crystalline basement of Archean to lower Proterozoic age (Luo, 1998; Yuan et al., 2000; Zhang et al., 2009; Zhao et al., 2011). Zhang et al. (2013) suggested the strong negative anomalies in the northwestern corner of the basin were caused by the folded uplift of local weak magnetic Feixianguan rocks (Zhang et al., 2013).

Besides the massive high anomaly in the northwestern half of the basin, some scattered positive anomalies can be also found in the west in the Ya'an-Wenchuan and Micangshan FTB areas (see white arrows in Figure 4.12). In Figure 2.2, these areas were mapped as Precambrian igneous intrusions. Thus, there is reason to believe that Precambrian igneous rocks are the major cause of many local magnetic anomalies. To further investigate the anomalies with the deep crustal configuration, a 40 km upward continuation was employed to the RTP grid in Figure 4.13.

Comparing Figure 4.13 and Figure 4.12, the northwest half of the basin is associated with a pronounced positive magnetic anomaly. The magnetic intensities in the southeastern half of the basin (outlined in white) are higher compared to Figure 4.12, suggesting that sources of the magnetic anomalies in the area are at a lower crustal depth. This also supports the previous hypothesis that a crystalline basement might exist beneath a large portion of the Sichuan Basin. In addition, the positive magnetic anomalies are not observed in Figure 4.13, especially in the Xichang and Micangshan FTB areas, which indicates that these local anomalies are caused by shallower magnetic bodies that can be explained by local igneous intrusions. Figure 4.14 was generated as a residual magnetic map of the study area, after subtracting the 40 km upward continuation grid from the RTP grid. Comparing Figures 4.12 and 4.14, the residual

magnetic map is highly consistent with the original RTP map, which clearly documents that in the study area, the magnetic anomalies are dominated by shallow crustal features. In addition, the magnetic anomalies are generally consistent with the NE orientation of the gravity anomalies.

4.3 Seismic Reflection Data Analysis

Raw SEGY format seismic data for three seismic profiles were made available for this study and were imported into the GeoGraphix data processing package for analysis (see Figure 3.2 for their locations). Based on well logging and other data, Dr. Xinguo Duan and his team interpreted all three seismic lines. The three approximately parallel seismic profiles are shown in three cross-sections respectively (Section A in Figure 4.15, Section B in Figure 4.16, and Section C in Figure 4.17). All of the profiles start at the foothills of the Longmenshan and extend southeast across the NW Depression in the basin. Section A is the longest, and crosses the core of the Central paleo-uplift and ends at the edge of the SE Depression. Section B starts closer to Longmenshan and ends at the edge of the Central paleo-uplift. Section C does not fully extend across the Central paleo-uplift. Section D in Figure 3.2 marks the location of the integrated gravity model shown in Figure 4.18 and is discussed in section 4.4.

On all three profiles, the most significant feature is the thick layer of Upper Triassic sediments, especially shown in Figure 4.15 (Symbolled as T_{3x}, Xujiahe Formation, ~3500 m thick). This predominant feature indicates that during Late Triassic time, the western Sichuan Basin started to subside, as a result of the impaction of the South China block and Songpan-Ganzi terrane. Xu et al. (1992) stressed that the South China block (SCB) deeply subducted westward beneath the Songpan-Ganzi terrane

during Late Indosinian orogeny in Late Triassic. The evidence of Longmenshan orogeny can be found from the remarkably thick Xujiahe sediments (Figure 4.15) as well as the well-developed normal faults in the NW Depression, shown as red lines (Figure 4.15 and Figure 4.16). Figure 4.17 documents that the thickness of all layers varies slightly in Section C, which indicates the Central paleo-uplift grew slightly toward northeast. Compared with the other two sections, fault system in the Section C also was not well developed.

In Figure 4.15, several major regional unconformities can be recognized along the Section A. 1) The Sinian reflectors unconformably overlapped on Pre-Sinian igneous rock or intrusions, which is the result of Jinning Movement. 2) The unconformity between Cambrian and Sinian is the evidence of Tongwan Movement. Also, the Cambrian layers get thinner over the Central paleo-uplift, suggesting the paleo-uplift was active during the Cambrian. 3) The Ordovician units unconformably overlapped on the Cambrian units during the Middle Caledonian Cycle, and the Ordovician sediments displays onlap features on the Cambrian units (see the lower right side of Figure 4.15). The top of Ordovician is truncated westward near the Longmenshan (see the lower left side of Figure 4.15). 4) The strata from Devonian and Silurian are missing, likely because this was the peak time of the Caledonian Orogeny. 5) Xujiahe (Upper Triassic)/Leikoupo (Middle Triassic) exhibits a disconformity, which is caused by the Early Indosinian Movement. 6) The contact between Triassic and Jurassic units is an angular unconformity, which is the result of Late Indosinian Movement.

Based on three lines of evidences, the inference can be made that the core of the Central paleo-uplift is located in the southwestern Sichuan Basin. First, in Section A, the different stratal thicknesses vary, particularly the Xujiahe Formation. In Section C, the stratal thickness is more uniform than those in Section A and B. This shows the development of the Central paleo-uplift is decreasing from south to north. Second, the fault systems developed in Section C are minor compared to the other two, which indicates that the development of the Central paleo-uplift is minor to the northeast. Third, the stratal depths in Section A are quite shallower than those of Section C, which also implies the paleo-uplift is higher in the southwest basin. In addition, the thickness of Xujiahe formation decreases from Section A to Section C suggesting that the foreland basin depocenter was also located in the southwest of Sichuan basin. In other word, if a cross-section is drawn more south than the other three, it will cross the depocenter of Xujiahe Formation and structurally highest portion of the paleo-uplift.

4.4 Integrated Geological Model

In order to quantitatively validate the interpretations that were discussed in previous chapters, a 2-D crustal-scale integrated geological model was constructed. Although this result is technically a gravity model, it is based on careful integration of geological, drilling, seismic reflection data, and the latest gravity data available to produce a result that satisfies all of the constraints.

As discussed in the seismic interpretation section, development of Longmenshan orogeny, Central paleo-uplift, and the foreland basin subsidence are centered in the southwest portion of the Sichuan basin. Thus, a cross-section through the core of Central paleo-uplift and perpendicular to the Longmenshan FTB was chosen (Section

D). It is much closer to the core tectonic evolution region than the three seismic profiles discussed, thus more geological features can be displayed by analyzing the 2-D integrated geological model of Section D (Figure 3.2). Based on 100 gravity data points extracted from the original CBA grid, a model was developed that demonstrates a density variation in different layers extending from the uppermost mantle up to the surface (Table 4.1). The densities of the units were derived from well-logging data in former studies (Lin and Zhu, 1993; Liu and Chang, 2003; Zhang., 2010; Jiang et al., 2012). Strata of Paleogene-Neogene, Devonian, and Silurian were not put into the model, since they are too thin or absent. Middle and Lower Triassic units have the same density value; thus, they were grouped into a single density layer.

The model was computed using trial and error matching of the observed and calculated values employing the GM-SYS profile modeling package in Oasis Montaj, which was shown in Figure 4.18. The key parameters iterated in the model were Moho depth, rock densities, and subsurface geology. With the use of the seismic reflection analysis and Dr. Xinguo Duan's unpublished geological interpretation for Section A, the depth and thickness variation of the sedimentary units are better constrained from Longmenshan foothill to the east edge of the Central paleo-uplift. The average Moho depth inside the basin is 42 ~ 45 km, with a trend of thinning toward the Songpan-Ganzi terrane to the Sichuan Basin (Deng et al., 1994; Song and Luo, 1995; Jiang et al., 2001; Zhang et al., 2010; Xu et al., 2016). The lower crust depth is 25 ~ 28 km, with a trend of thinning underneath the Central paleo-uplift (Deng et al., 1994; Zhang et al., 2010; Xu et al., 2016). The depth of the upper crust (basement) slightly shallows underneath the Central paleo-uplift forming a domal geometry in Figure 4.18. Meanwhile, the

sedimentary strata are up-warped in the Central paleo-uplift area, which coincides with the deformation of the deep basin structure, suggesting the Central paleo-uplift has undergone multiple stages development. In stark contrast, Longmenshan FTB is a much more complex geologic structure, in which a fragmented upper crust can be seen in Figure 4.18. Faults are well developed at depth, and older formations are thrust over younger formations. The intense Longmenshan deformation played a major role in the development of the NW Depression, which provided space for the thickest accumulation of the Xujiahe Formation in the Late Triassic.

Chapter 5. Discussion and Conclusions

This thesis has integrated former research achievements and newly collected data, and generated a series of gravity and magnetics anomaly maps, which served the goal of advancing interpretations of the regional tectonic evolution and its implications for understanding destructive earthquakes and growing gas exploration in this region. There are three main results of this thesis: First is the integrative analysis of three long seismic reflection profiles, which helps clarify the relationships of the Longmenshan FTB and the Central paleo-uplift, and provides better control of the depth and thickness variations of sedimentary units in the NW Depression. On the contrary, previous researchers usually grouped all the Cambrian-Quaternary sediments as one layer in their density model. The second is that the potential field data derived from the latest databases provide a set of higher resolution gravity and magnetic anomaly maps. These maps help define the crustal structure in 3-D and contribute to the construction of the integrated 2-D model. The third is that former studies in Sichuan Basin are focused on the Longmenshan region and NW Depression, while the 2-D model derived in this thesis extends eastward to the SE Depression and constructed a crustal-scale profile across the Sichuan Basin.

This thesis supports the viewpoint that the Central paleo-uplift has experienced two stages of deformation: the Leshan-Longnvsi paleo-uplift during the Caledonian orogeny (Ordovician – Early Devonian) and the Luzhou-Kaijiang paleo-uplift during the Indosinian orogeny (Late Permian – Triassic). In addition, comparison of residual gravity and magnetic maps in different depths helped in the investigation of the deep

structural configuration, such as the paleo-uplift and deep crustal layers down to the Moho.

The Late Triassic witnessed the Longmenshan orogeny and the second stage of the Central paleo-uplift, during which the Sichuan Basin was transformed into a terrestrial lacustrine basin. This transformation had important influence on the foreland basin from two aspects. On one hand, Longmenshan FTB became an extremely unstable geologic disaster-prone area since the collision of the Songpan-Ganzi terrane and the South China block. For instance, in city of Ya'an area, two gravity gradient belts converge and subsequent strong earthquakes occurred after the Wenchuan earthquake over several years. On the other hand, the formation of western Sichuan foreland basin provided an excellent accommodation space for deposition of the Xujiahe Formation. The depocenter of Late Triassic sediments is located in the southwest portion of the basin, adjacent to the core of the paleo-uplift. The depocenter and the uplift have been developed into large gas fields, such as Xinchang and Hechuan fields. It is an earthquake-prone region, but nevertheless, it bears great potential for natural gas reservoirs.

The integrated model extends across the SE Depression, which provides a 2-D crustal-scale picture of the southeast basin. Sediments from Triassic and Jurassic are also abundant in the SE depression, indicating it may be gas-rich and thus a good exploration target for further consideration.

References

Amante, C., Eakins, B.W., 2009, ETOPO1: 1 arc-minute global relief model: procedures, data sources and analysis, NOAA Tech. Mem. NESDIS NGDC24, Boulder(Co).

Andersen, O., 2010, The DTU10 Global Gravity field and mean sea surface – improvements in the Arctic. 2nd IGFS meeting, Fairbanks, Alaska, Sept. 2010.

Blakely, R. J., 1996, Potential theory in gravity and magnetic application: Cambridge, UK, Cambridge University Press, p.441.

Bonvalot, S., Balmino, G., Briais, A., M. Kuhn, Peyrefitte, A., Vales N., Biancale, R., Gabalda, G., Reinquin, F., Sarrailh, M., 2012, World Gravity Map. Commission for the Geological Map of the World, Eds. BGI-CGMW-CNES-IRD, Paris.

Burchfiel, B. C., Z. Chen, Y. Liu, and L. H. Royden, 1995, Tectonics of the Longmen Shan and adjacent regions, central China: International Geology Review, v. 37, p.661-735.

Cai, C., Worden, R. H., Bottrell, S. H., Wang, L., Yang, C., 2003, Thermochemical sulphate reduction and the generation of hydrogen sulphide and thiols (mercaptans) in Triassic carbonate reservoirs from the Sichuan Basin, China: Chemical Geology, v. 202, p.39-57.

Chen, S., Deng, Q., Zhao, X., Dirks, C. J., Luo L., Liu, S., 1994, Deformational characteristics, evolutionary history, and deformation mechanism of the middle Longmenshan thrust-nappes and related tectonics: Seismology and Geology, v. 16, no. 4, p.404-421.

Chen, S, and Wilson, C. J. L., 1996, Emplacement of the Longmen Shan thrust-nappe belt along the eastern margin of the Tibetan Plateau: Journal of Structure Geology, v. 18, p.413-430.

Chen, Z., Jia, D., Zhang, Q., Wei, G., Li, B., Wei, D., Shen, Y., 2005, Balanced cross-section analysis of the fold-thrust belt of the Longmen Mountains: Acta Geologica Sinica, v. 79, p. 38-45.

Cheng, Y., 1990, Geological map of China: Beijing, Geological Publishing House, scale 1: 4,000,000.

Deng, Q., Chen, S., Zhao X., 1994, Tectonics, Seismicity and dynamics of Longmenshan Mountains and its adjacent regions: Seismology and Geology, v.27, no.4, p.389-403.

Department of Civil Affairs of Sichuan Province, 2013, http://www.scmz.gov.cn/InfoDetail.asp?ID=12210

Dong, S., Hu, J., Shi, W., Zhang, Z., Liu G., 2006, Jurassic superposed folding and Jurassic foreland in the Data Mountain, Central China: Acta Geoscientica Sinica, v.27, no.5, p.403-410.

Dong, S., Shi, W., Zhang Y., Hu J., Zhang, Z., Li, J., Wu, H., 2010, The tectonic stress field in the Dabashan Orogen resulting from late Mesozoic intra-continental orogeny, Acta Geoscientica Sinica, v.31, no.6, p.769-780.

Frey, H., 1982, MAGSAT scalar anomaly distribution: the global perspective: Geophysical Research Letters, v. 9, no. 4, p.277-280.

Fu, X., Hou, W., Li, H., Wang, Z., Zou, F.,2008, Coseismic Deformation of the Ms 8.0 Wenchuan Earthquake and its relationship with Geological Hazards, Acta Geologica Sinica, v.82, no.12, p.1733-1746.

GeoForschuangsZentrum, 2016, http://www.gfz-potsdam.de/301/

Getech, 2016, http://www.getech.com/gravity-magnetic/

Hao, F., Guo, L., Zhu, Y., Cai, X., Zou, H., Li, P.,2008, Evidence for 121 multiple stages of oil cracking and thermochemical sulfate reduction in the Puguang gas field, Sichuan Basin, China: American Association of Petroleum Geologist Bulletin, v. 92, p. 611–637.

He, D., Li, D., Zhang, G., Zhao L., Fan, C., Lu, R., Wen, Z., 2011, Formation and evolution of multi-cycle superposed Sichuan Basin, China: Chinese Journal of Geology, v. 46, no. 3, p.589-606.

Heiskanen, V.A., Moritz, H,1967, Physical Geodesy, San Francisco: W.H. Freeman and Company, p.364.

Holom, E. R., Oldow, J. S., 2007, Gravity reduction spreadsheet to calculate the Bouguer anomaly using standardized methods and constants: Geosphere v. 3, p. 86-90.

Huang, J., Chen, B., 1987, The evolution of the Tethys in China and its adjacent regions: Beijing, Geologic Publishing House, p. 109.

Huang, X., Xie, F., 2009, Review of the evolutionary history and tectonic style of Longmenshan Tectonic Belt: Crust structure and crust stress corpus (21), CNEC, p. 16-29.

Jia, D., Wei, G., Chen, Z., Li, B., Zeng, Q., Yang., G., 2006, Longmen Shan fold-thrust belt and its relation to the western Sichuan Basin in central China: New insights from hydrocarbon exploration: American Association of Petroleum Geologists Bulletin, v. 90, no. 9, p. 1425-1447.

Jiang, W., Liu, Y., Hao, T., Song, H., 2001, Comprehensive study of geology and geophysics of Sichuan Basin: Progress in Geophysics, v.16, no.1, p. 11-23.

Jiang, W., Zhang, J., Tian, T., Wang, X., 2012, Crustal structure of Chuan-Dian region derived from gravity data and its tectonic implications: Physics of the Earth and Planetary Interiors, v. 212-213, p. 76-87.

Keller, G. R., Hildenbrand, T. G., Kucks, R., Roman, D., Hittleman, A. M., 2002, Upgraded gravity anomaly base of the United States: The Leading Edge, v. 21, no. 4, p. 366-367.

Keller, G. R., Hildenbrand, T, G., Kucks, R., Webring, M., Briesacher, A., Rujawitz, K., Hittleman, A.M., Roman, D.J., Winester, D., Aldouri, R., Seeley, J., Rasillo, J., Torres, T., Hinze, W.J., Gates, A., Kreinovich, V., and Salayandia, L., 2006, A community effort to construct a gravity database for the United States and an associated Web portal. In: A. K. Sinha, Editor. Geoinformatics: Data to Knowledge, Geological Society of America Publ., Boulder, Colorado, p. 21-34.

Li, L., 2011, Shale gas exploration and development status in Sichuan Basin: China National Petroleum Company internal conferences.

Li, X., Götze, H.J., 2001, Ellipsoid, geoid, gravity, geodesy and geophysics: Geophysics, v.66, no.6, p.1660-1668.

Lin, T., Zhu, H., 1993, Physical Property of Pre-Cretaceous Rocks in the Sichuan Basin, China: Geoinformatics, v. 4, no. 3, p. 337-346.

Liu, S., Luo, Z., Dai, S., Arne, D., and Wilson, C.J.L., 1995, The uplift of the Longmenshan thrust belt and subsidence of the western Sichuan foreland basin: Acta Geologica Sinica, v.69, n.3, p.205-214.

Liu, Y., Chang, X., 2003, Modeling of Burial and subsidence history in Sichuan Basin: Chinese Journal of Geophysics, v. 46, no. 2, p. 203-208.

Luo, Z., 1991, The dynamical model of the lithospheric evolution in Longmen Shan orogenic belt: Journal of Chengdu College of Geology, v. 18, p. 1-7.

Luo, Z., 1998, New recognition of basement in Sichuan Basin: Journal of Chengdu University of Technology, v. 25, p. 191-200.

Luo, Z., and Long, X., 1992, The uplift of Longmen Shan orogenic zone and subsidence of the western Sichuan foreland basin. Acta Geologica Sichuan, v. 12, p. 1-17.

Luo, Z., Liu, S., Liu, S., Yong, Z., Zhao, X., Sun, W., 2004, The action of “Emei Mantle Plume” on the separation of the Yangtze Plate from the Tarim Plate and its significance in exploration: Acta Geoscientica Sinica, v. 25, no. 5, p. 515-522.

Ma, Y., Cai, X., Zhao, P., Luo, Y., Zhang, X., 2010, Distribution and further exploration of the large-medium sized gas fields in Sichuan Basin: Acta Petrolei Sinica, v. 31, no. 3, p. 347-354.

Ma, Y., Guo, X., Guo, T., Huang, R., Cai, X., Li, G., 2007, The Puguang gas field - New giant discovery in the mature Sichuan Basin, southwest China: American Association of Petroleum Geologist Bulletin, v. 91, no. 5, p. 627-643.

Meng, Q., Wang, E., Hu, J., 2005, Mesozoic sedimentary evolution of the northwest Sichuan basin: Implication for continued clockwise rotation of the South China Block: Geological Society of America Bulletin, v. 117, no. 3/4, p. 396-410.

Meng, Q., Zhang, G., 1999, Timing of collision of the North and South China blocks: Controversy and reconciliation: Geology, v. 27, p. 123-126.

Sichuan Bureau of Geology and Mineral Resources, 1991, Regional Geology of Sichuan Province. Beijing: Geological Publishing House, p. 1-680.

Sichuan Provincial People's Government, 2009, http://www.sc.gov.cn/zwgk/zwdt/bmdt/200905/t20090507_722124.shtml

Song, H., Luo, L., 1995, Research progress of Sichuan Basin basement and its deep geological structure: Earth Science Frontiers, v.2, no.3~4, p. 231-236.

Wang, B., 1989, The Sichuan hydrocarbon province: Petroleum geology of China: Beijing, Petroleum Industry Press, v. 10, p. 516.

Wang, J., Bao, C., Luo, Z., Guo, Z., 1989, Formation and development of the Sichuan Basin, in: Chinese Sedimentary Basins, Elsevier, p. 147-163.

Wang, Z., Zhao, W., Zhang L., Wu, S., 2002, The structural sequence of the Sichuan Basin and natural gas exploration: Beijing, Geological Publishing House, p. 287.

Xu, X., Gao, R., Guo, X., Keller, G. R., 2016, The crustal structure of the Longmen Shan and adjacent regions: An integrated analysis of seismic profiling and gravity anomaly, Chinese Journal of Geology, v. 51, no.1, p. 26-40.

Xu, Z., Hou, L., Wang, Z., Fu, X., Huang, M., 1992, Orogenic processes of the Songpan-Ganzi orogenic belt of China (in Chinese): Beijing, Geological Publishing House, 190 p.

Yin, H., Nie, S., 1996, A Phanerozoic palinspastic reconstruction of China and its neighboring regions, Tectonic Evolution of Asia: Cambridge, Cambridge University Press, p.442-485.

Yuan, X., Egorov, A., 2000, A short introduction to global geoscience transect 21: Arctic Ocean–Eurasia–Pacific Ocean. Science Press, Beijing.

Zhao, Y., Liu, L., Wang, S., Ren, Y., 2011, Data processing and interpretation of aeromagnetic and satellite magnetic survey in Longmen Mountain and its adjacent areas: Chinese Journal of Engineering Geophysics, v. 8, no. 5, p. 560-565.

Zhang, J., Gao, R., Zeng, L., Li, Q., Guan, Y., He, R., Wang, H., Lu, Z., 2009, Relationship between characteristics of gravity and magnetic anomalies and the earthquakes in Longmenshan range and adjacent areas: Chinese Journal of Geophysics, v. 52, no. 2, p. 572-578.

Zhang, J., Gao, R., Zeng, L., Li, Q., Guan, Y., He, R., Wang, H., Lu, Z., 2010, Relationship between characteristics of gravity and magnetic anomalies and the earthquakes in the Longmenshan range and adjacent areas: Tectonophysics, v. 491, p. 218-229.

Zhang, J., Gao, R., Zeng, L., Li, Q., Guan, Y., Wang, H., Li, W., 2013, Characteristic of gravity and magnetic anomalies in the Daba Shan and the Sichuan basin, China: Implication for Architecture of the Daba Shan: Acta Geologica Sinica (English Edition), v. 87, no. 4, p. 1154-1161.

Zhang, R., Niu, D., Huo, Y., Li, Y., and Zhang, L., 1992, Geologic map of Qinling-Daba Mountains and adjacent region of People's Republic of China: Beijing, Geological Publishing House, scale 1: 1,000,000.

Appendix: Figures and Tables

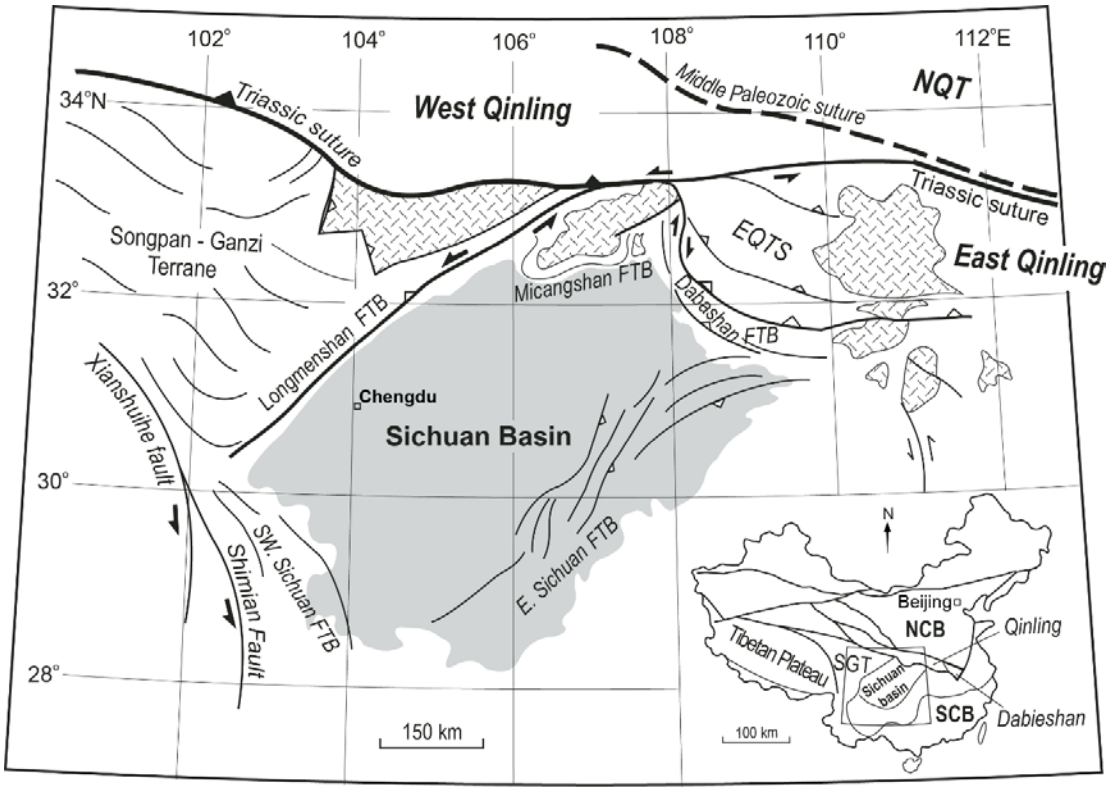

Figure 2.1. Simplified tectonic map of the Sichuan Basin and adjacent regions. Inset shows main tectonic elements of China. NCB-North China block, SCB-South China block, SGT-Songpan-Ganzi terrane, NQT-North Qinling terrane, EQTS-East Qinling thrust system, FTB-fold-thrust belt. Modified from Cheng, 1990, Zhang et al., 1992, and Meng et al., 2005.

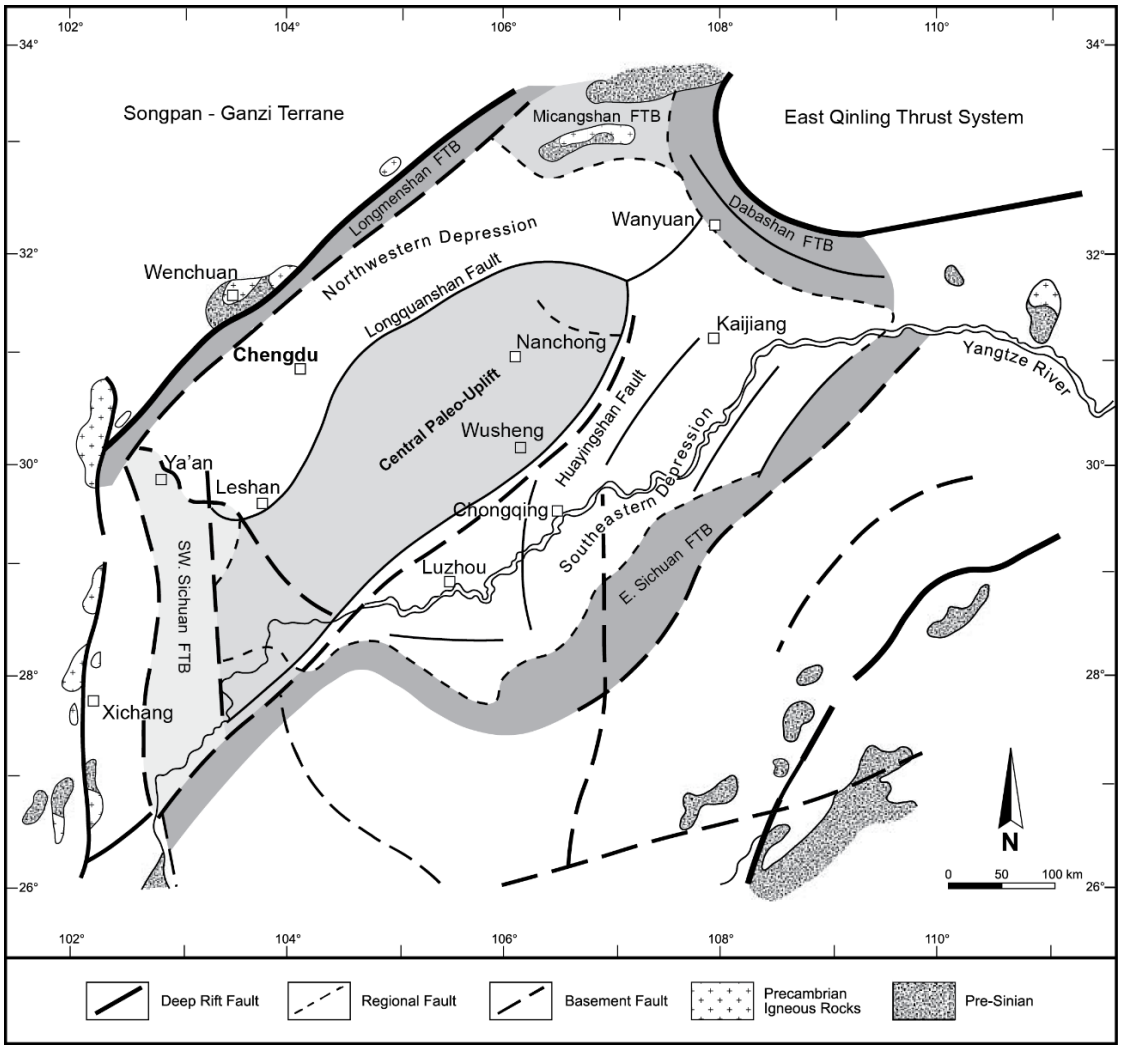

Figure 2.2. Structural configuration and subdivisions of the Sichuan Basin. FTB-fold-thrust belt. Modified from Wang et al., 1989; Ma et al., 2007.

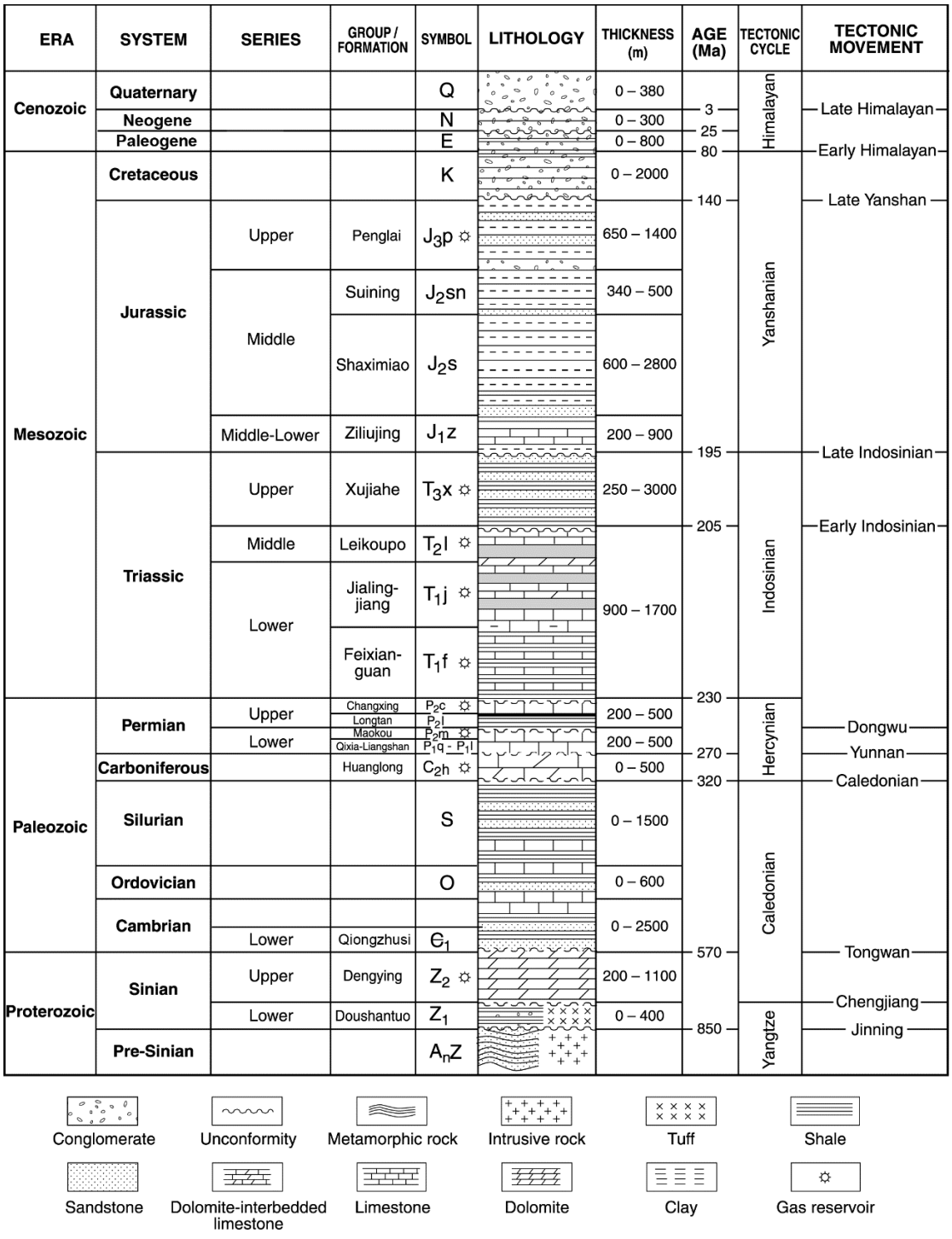

Figure 2.3. Generalized stratigraphy and tectonic history of the Sichuan Basin. Modified from Wang et al., 1989; Ma et al., 2007.

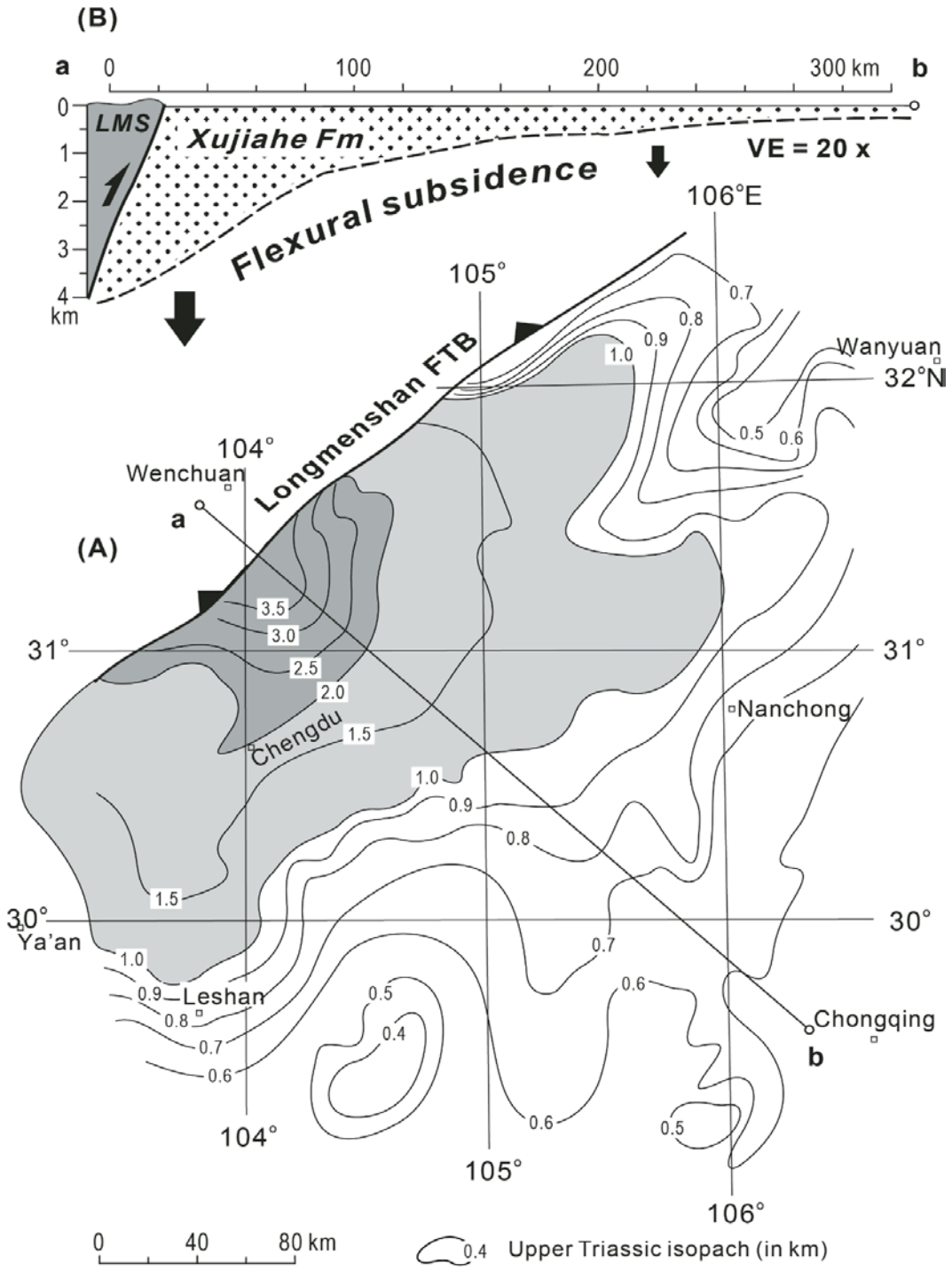

Figure 2.4. Isopach map of Upper Triassic Xujiahe Formation in the Sichuan Basin (A) and schematic cross-section (B). LMS-Longmenshan. Modified from Guo et al., 1996; Meng et al., 2005.

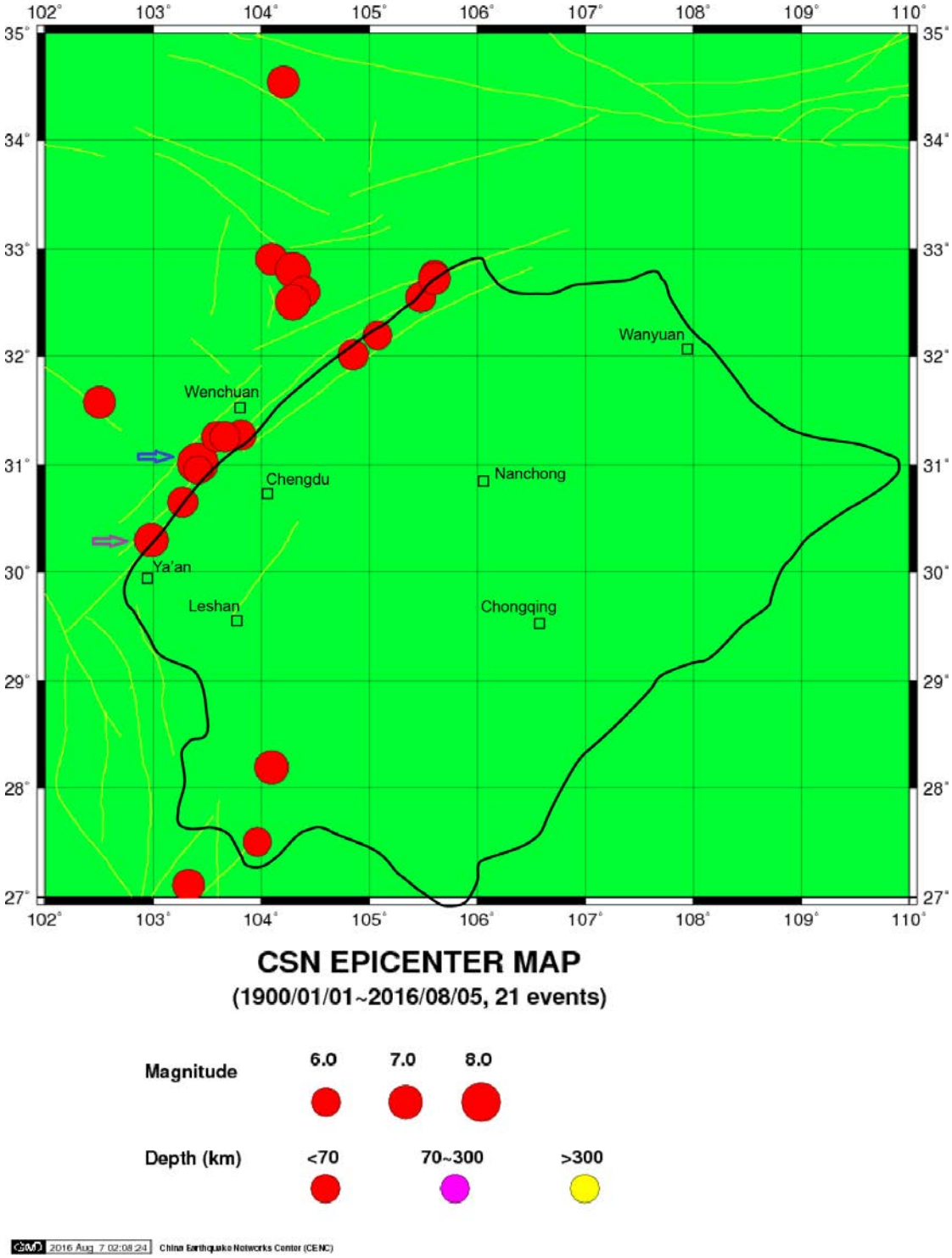

Figure 2.5. Historical seismicity map (>Ms 6.0) of the Sichuan Basin from 1900 to 2016. Data courtesy of China Earthquake Network Center (CENC). Note that the outline of the Sichuan Basin is marked in black lines.

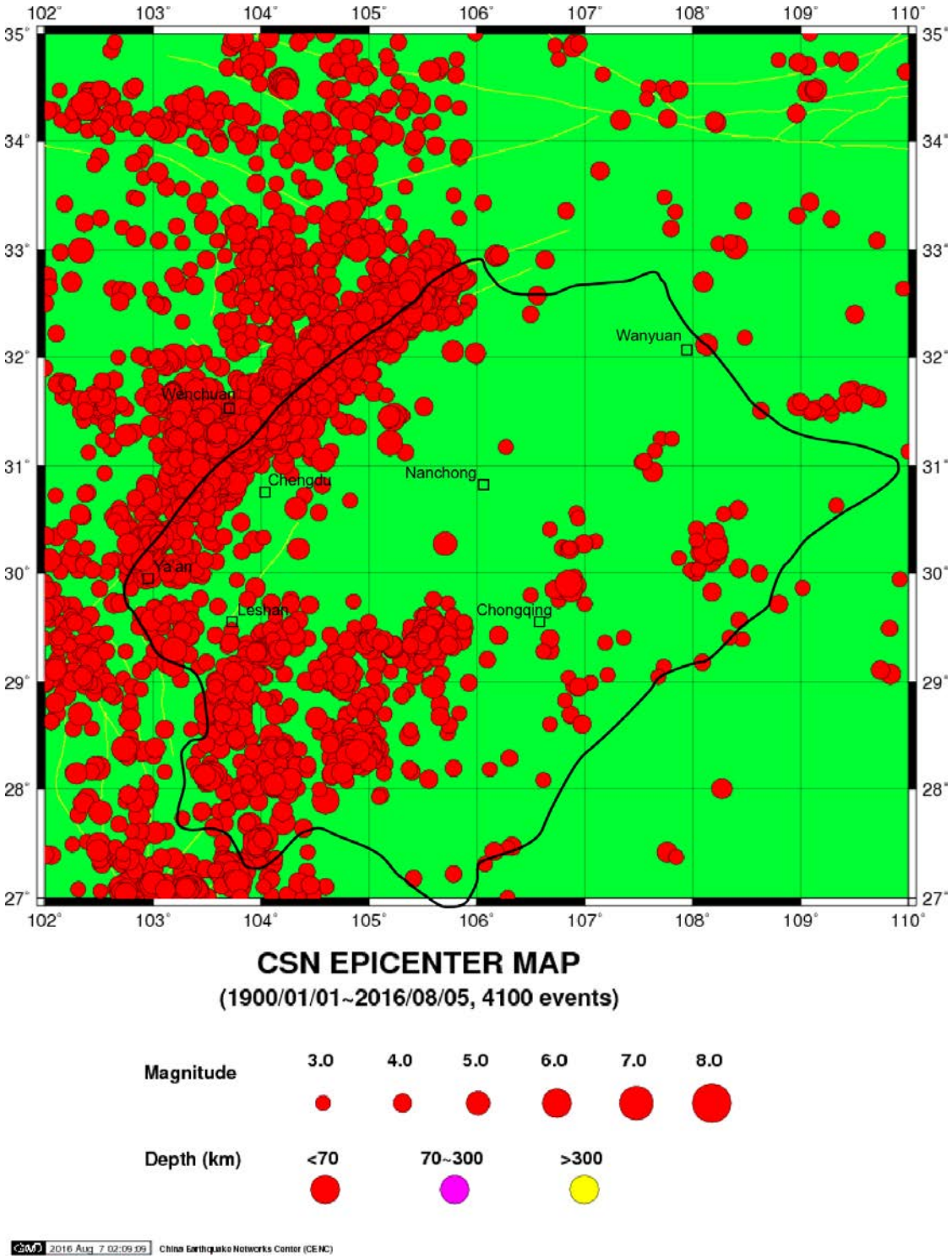

Figure 2.6. Historical seismicity map (>Ms 3.0) of the Sichuan Basin from 1900 to 2016. Data courtesy of China Earthquake Network Center (CENC). The map symbols are the same as Figure 2.5.

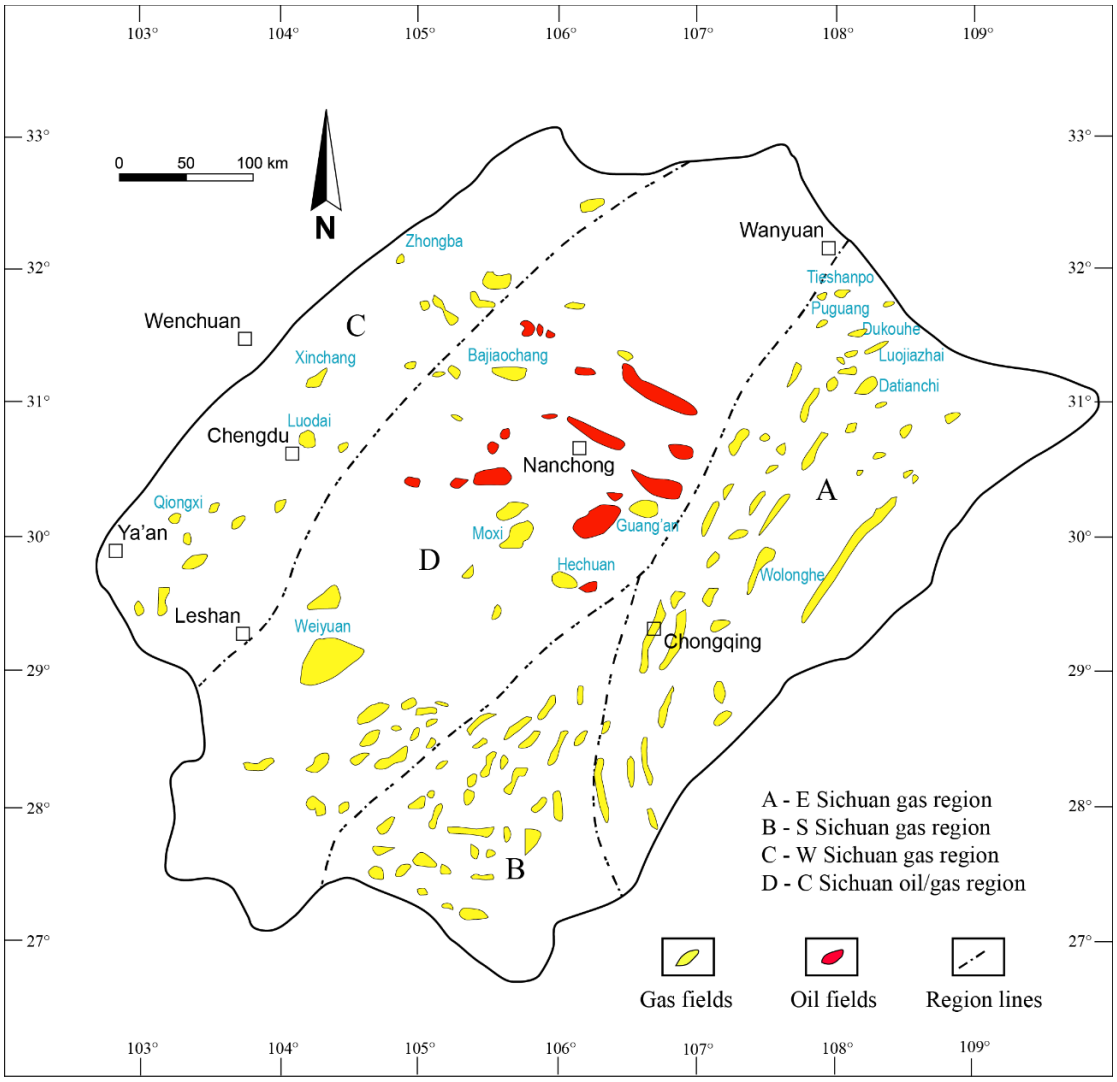

Figure 3.1. The location of oil and gas fields in Sichuan Basin. Note that the outline of the Sichuan Basin is marked in black lines. Large gas fields are labeled in blue. Modified from Ma et al., 2010.

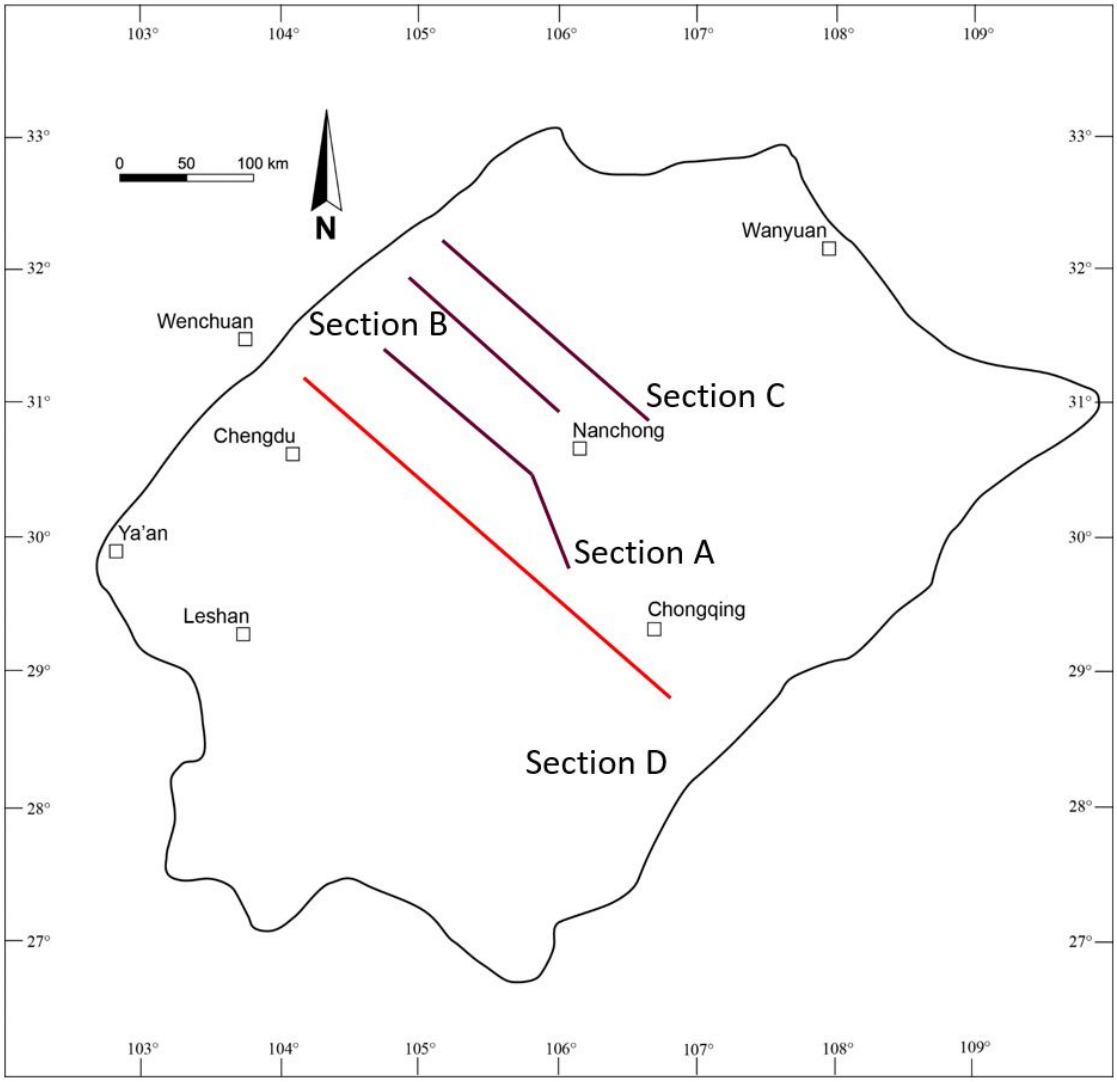

Figure 3.2. Index map of Sichuan Basin 2-D seismic profiles in brown lines (Section A, B, C), and 2-D model profile in red line (Section D). Modified from Ma et., 2010.

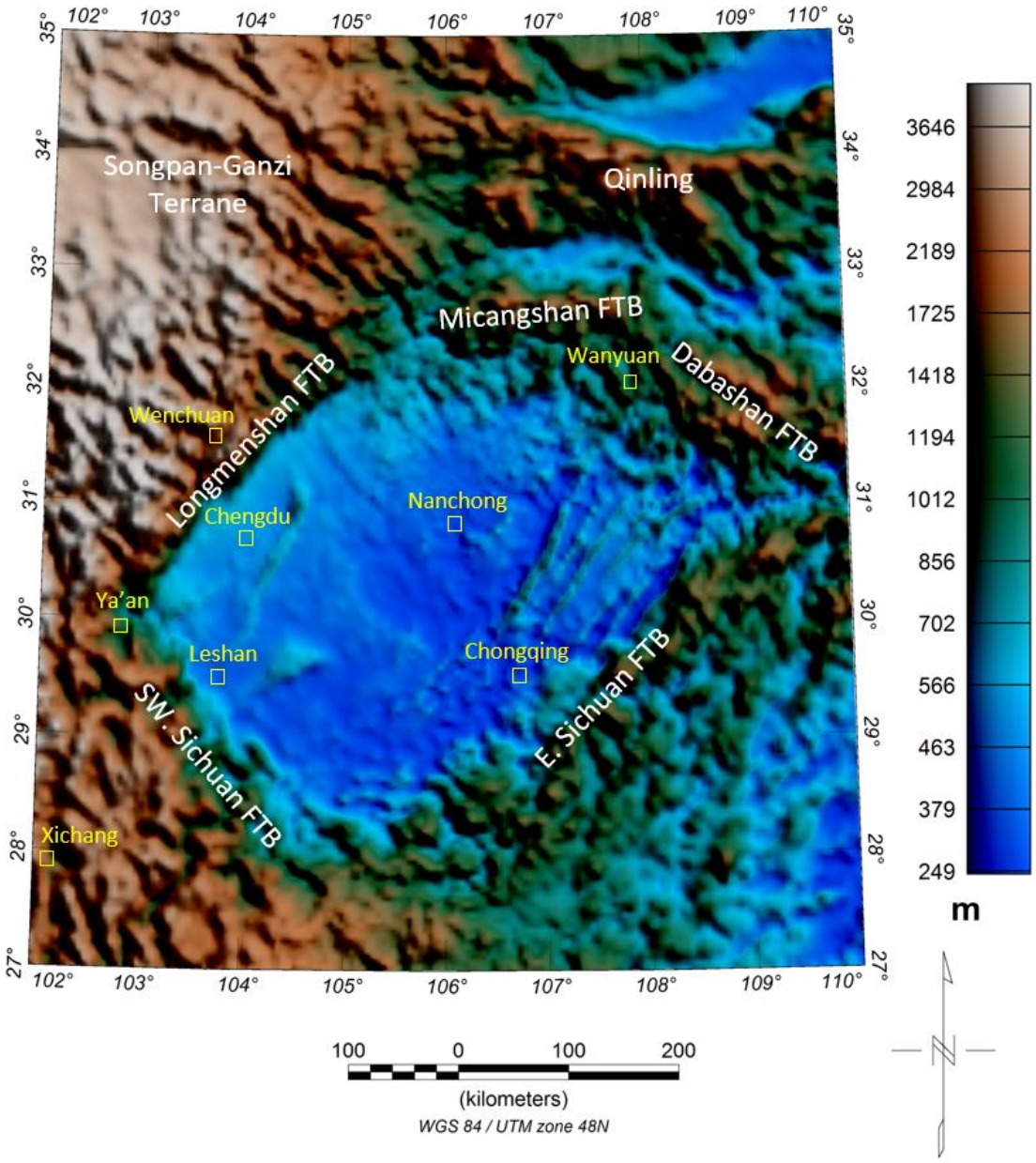

Figure 4.1. Digital Elevation Model (DEM) showing the topography of the Sichuan Basin. All DEM data courtesy of WGM 2012 project. The Sichuan Basin is surrounded with notable highs, especially in northwest Songpan-Ganzi terrane. FTB-fold-thrust belt.

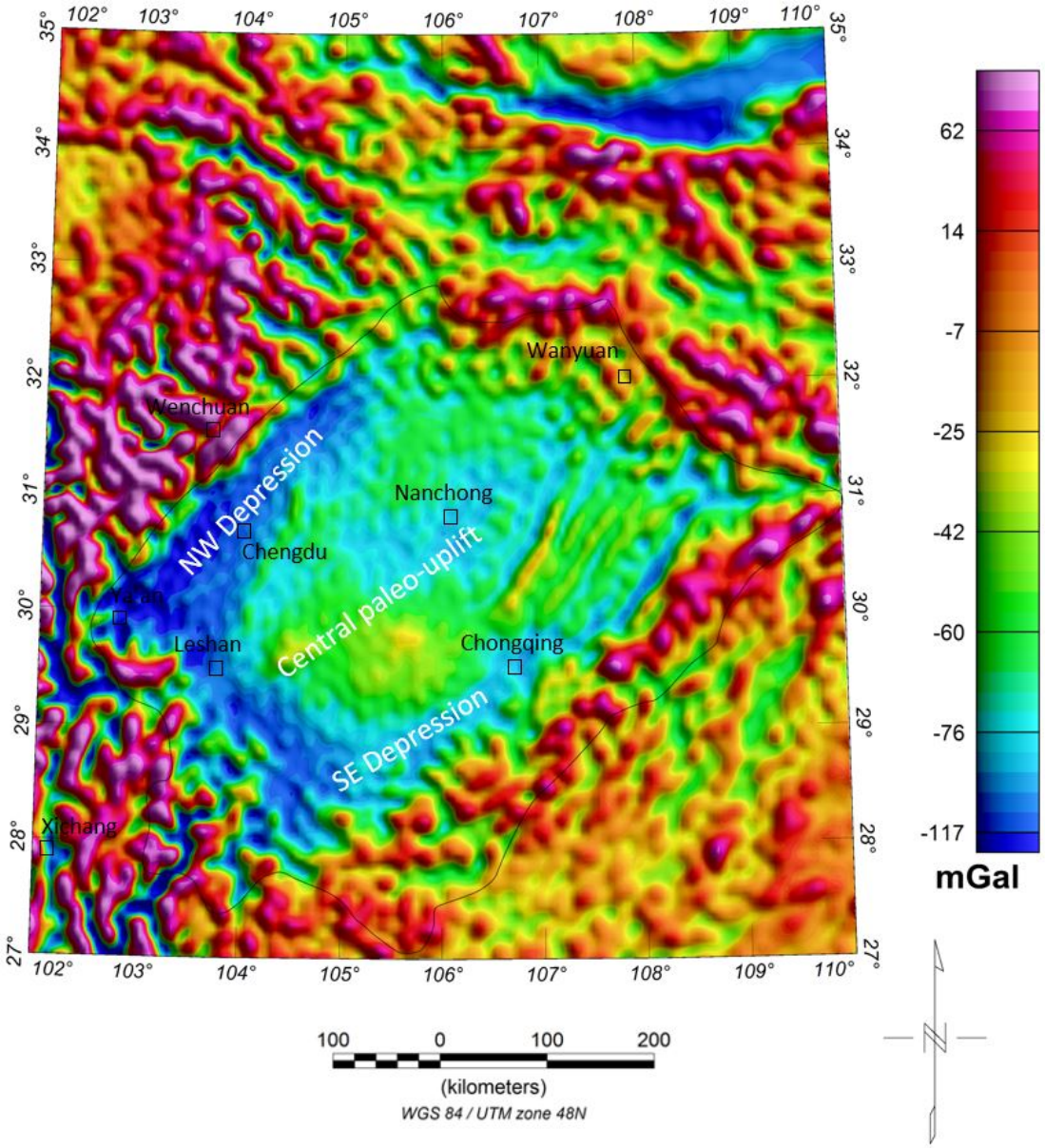

Figure 4.2. Free Air gravity anomaly map of the Sichuan Basin, outlined by black line. All gravity data courtesy of WGM 2012 project. Note that the outline of the Sichuan Basin is marked in black lines. The map symbols are the same as Figure 4.1.

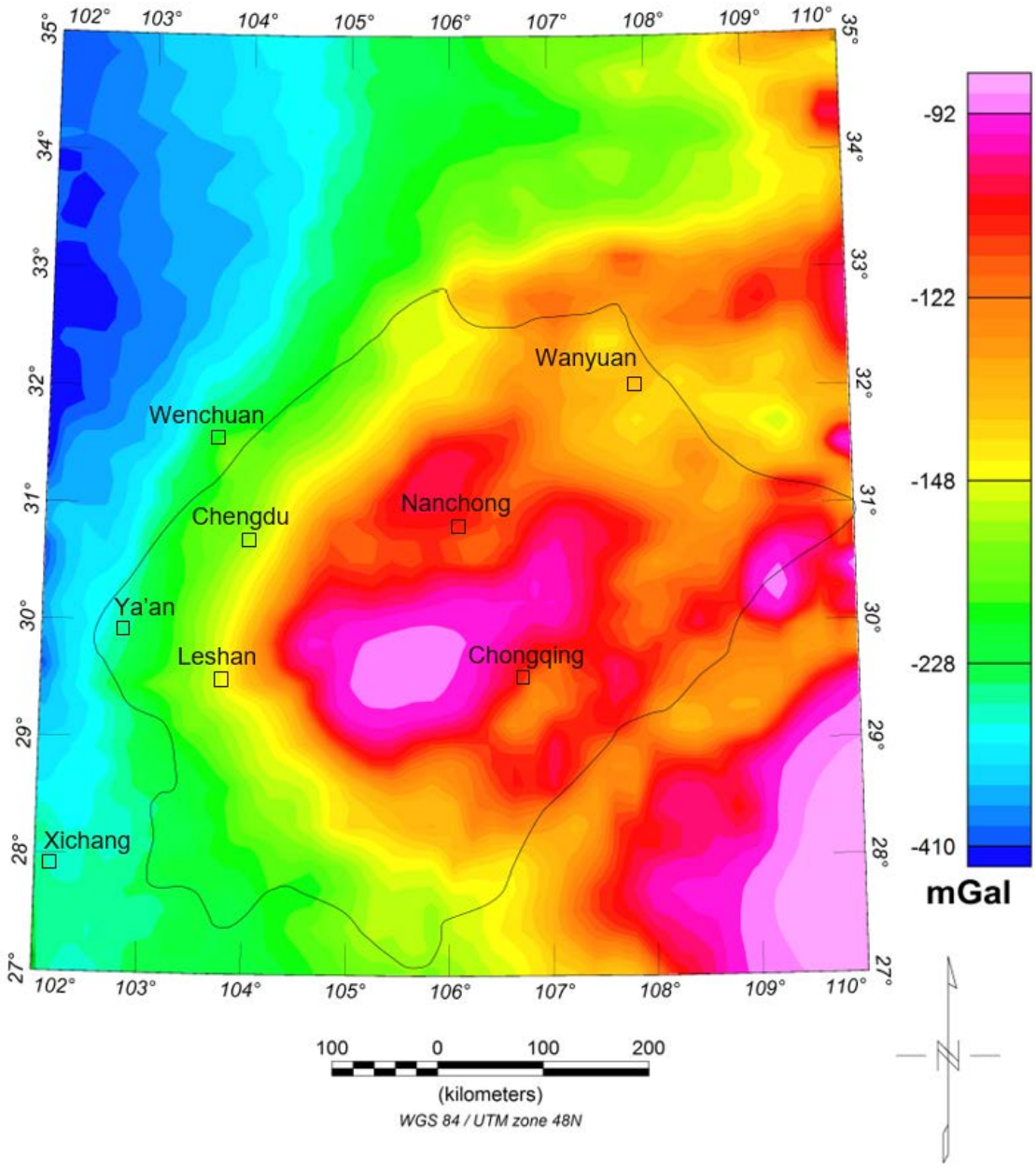

Figure 4.3. Complete Bouguer Anomaly (CBA) of the Sichuan Basin, shown in histogram color scheme. As defaulted in Oasis Montaj, a histogram map accentuates values of anomalies. The map symbols are the same as Figure 4.1.

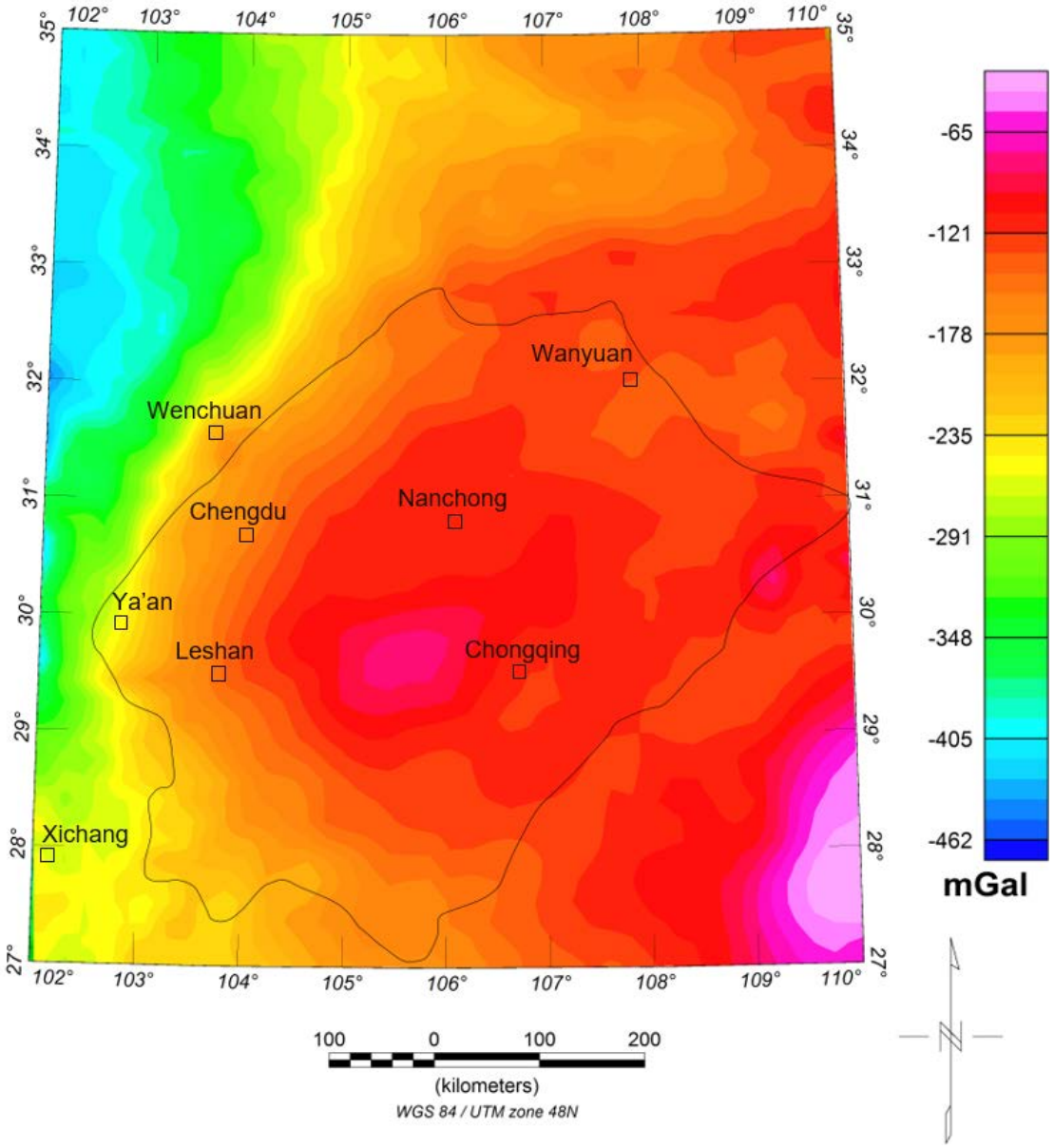

Figure 4.4. Complete Bouguer Anomaly (CBA) of the Sichuan Basin, shown in linear color scheme. Compared to the histogram map (default in Oasis Montaj), the linear map better represents transitions between anomalies. The map symbols are the same as Figure 4.1.

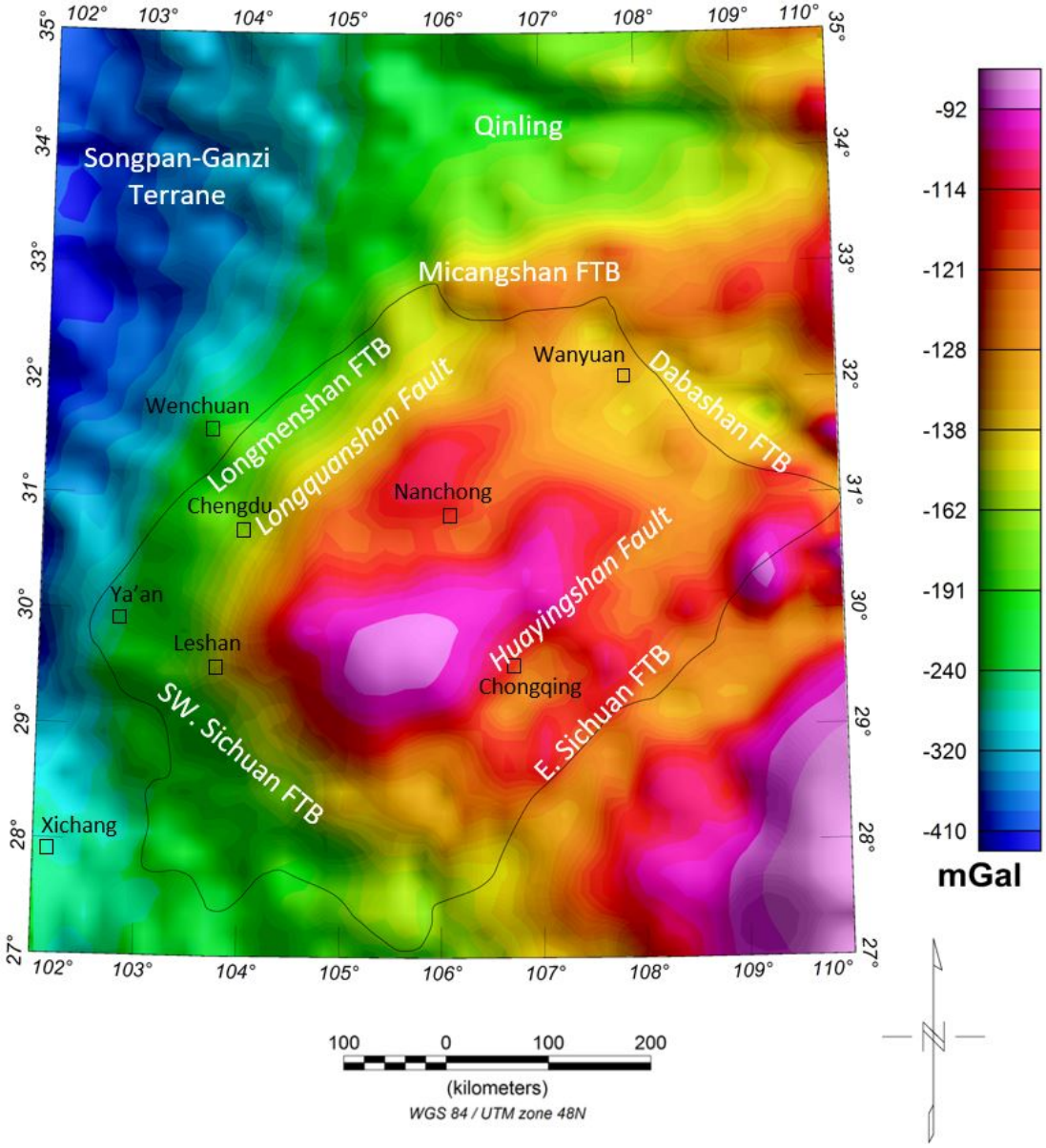

Figure 4.5. Complete Bouguer Anomaly (CBA) of the Sichuan Basin, shown in histogram color scheme, co-rendered with color shaded relief grid. The Sichuan Basin is situated in areas with pronounced negative anomalies, with a diamond shape. The maximum gravity high locates between Leshan and Chongqing. FTB-fold-thrust belt. The map symbols are the same as Figure 4.1.

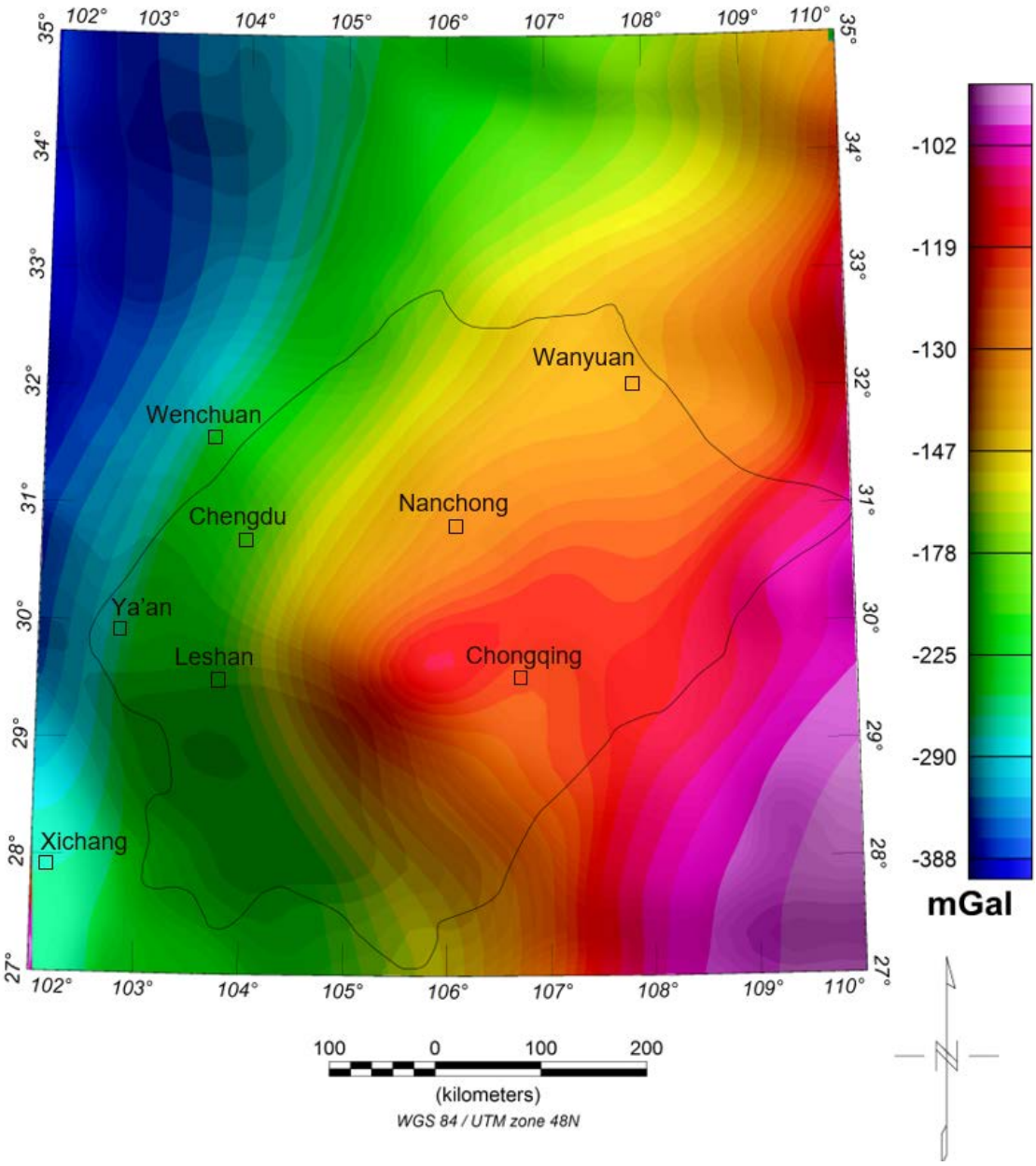

Figure 4.6. 40 km upward continuation of the Complete Bouguer Anomaly (CBA) map of the Sichuan Basin. Note that west of Chongqing still possesses that highest gravity anomaly inside the basin. In addition, Longmenshan and Southwest Sichuan FTB are vividly mapped in green belts. The map symbols are the same as Figure 4.1.

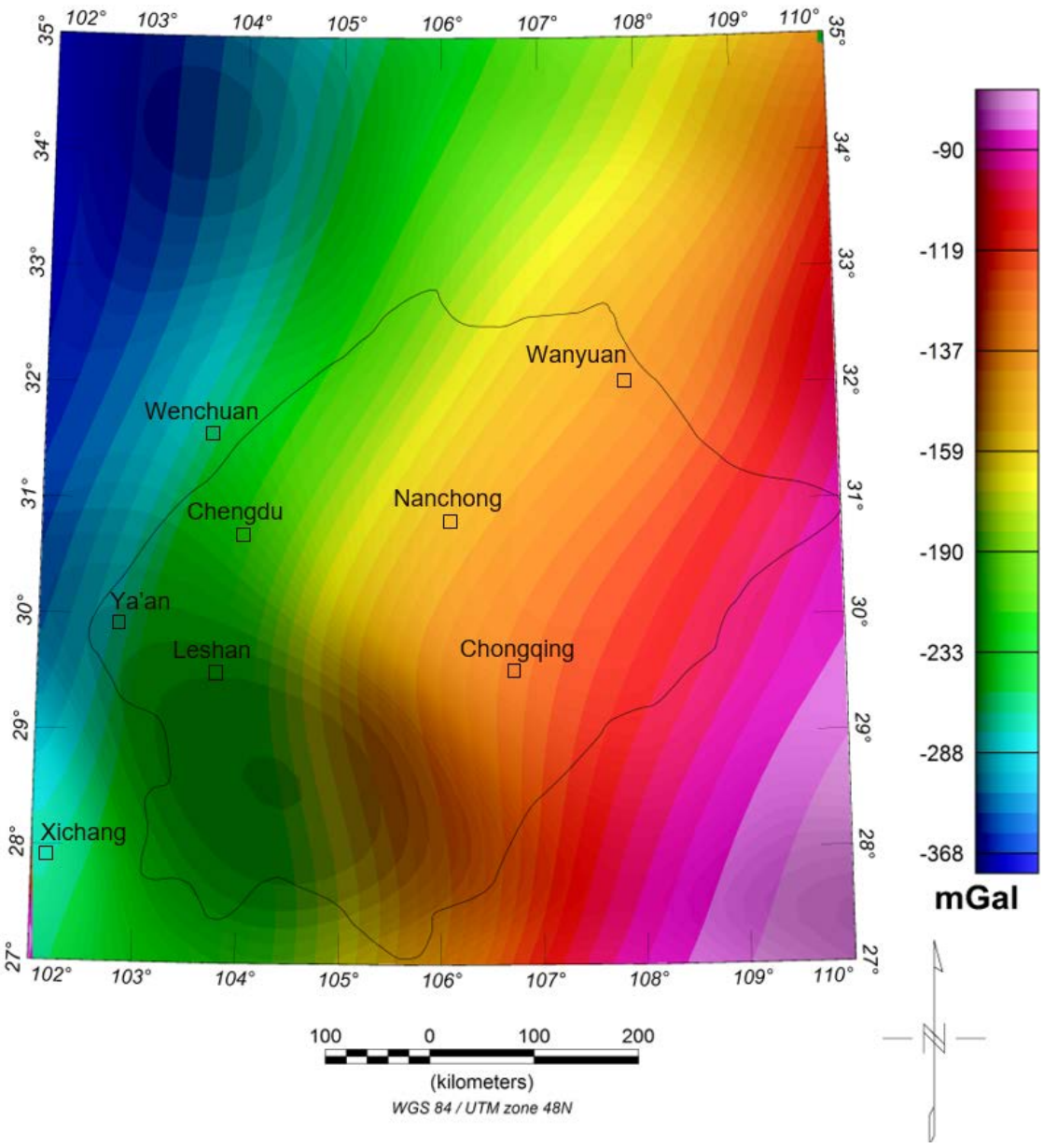

Figure 4.7. 100 km upward continuation of the CBA map of the Sichuan Basin. Comparing with 40 km upward continued map, the strong NW-SE increase in anomaly values primarily reflects the southeastward thinning of the crust. The map symbols are the same as Figure 4.1.

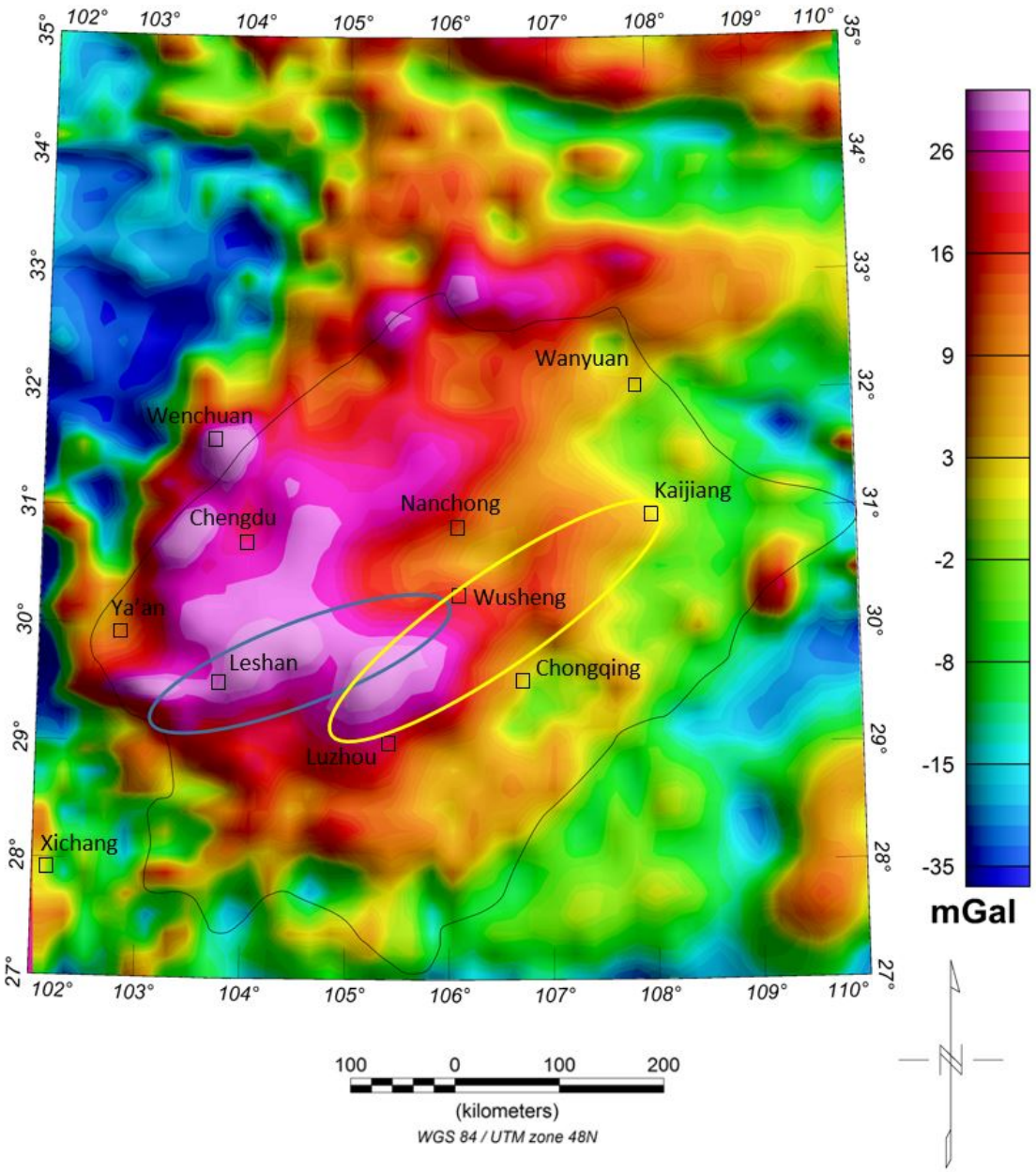

Figure 4.8. Residual gravity anomaly map of the Sichuan Basin, by subtracting the 40 km upward continued grid from the CBA grid. Note that the two gravity highs locate in Leshan and north Luzhou. The Leshan-Longnvsi (Wusheng) paleo-uplift is identified in blue circle, while the Luzhou-Kaijiang paleo-uplift is demonstrated in yellow circle. The map symbols are the same as Figure 4.1.

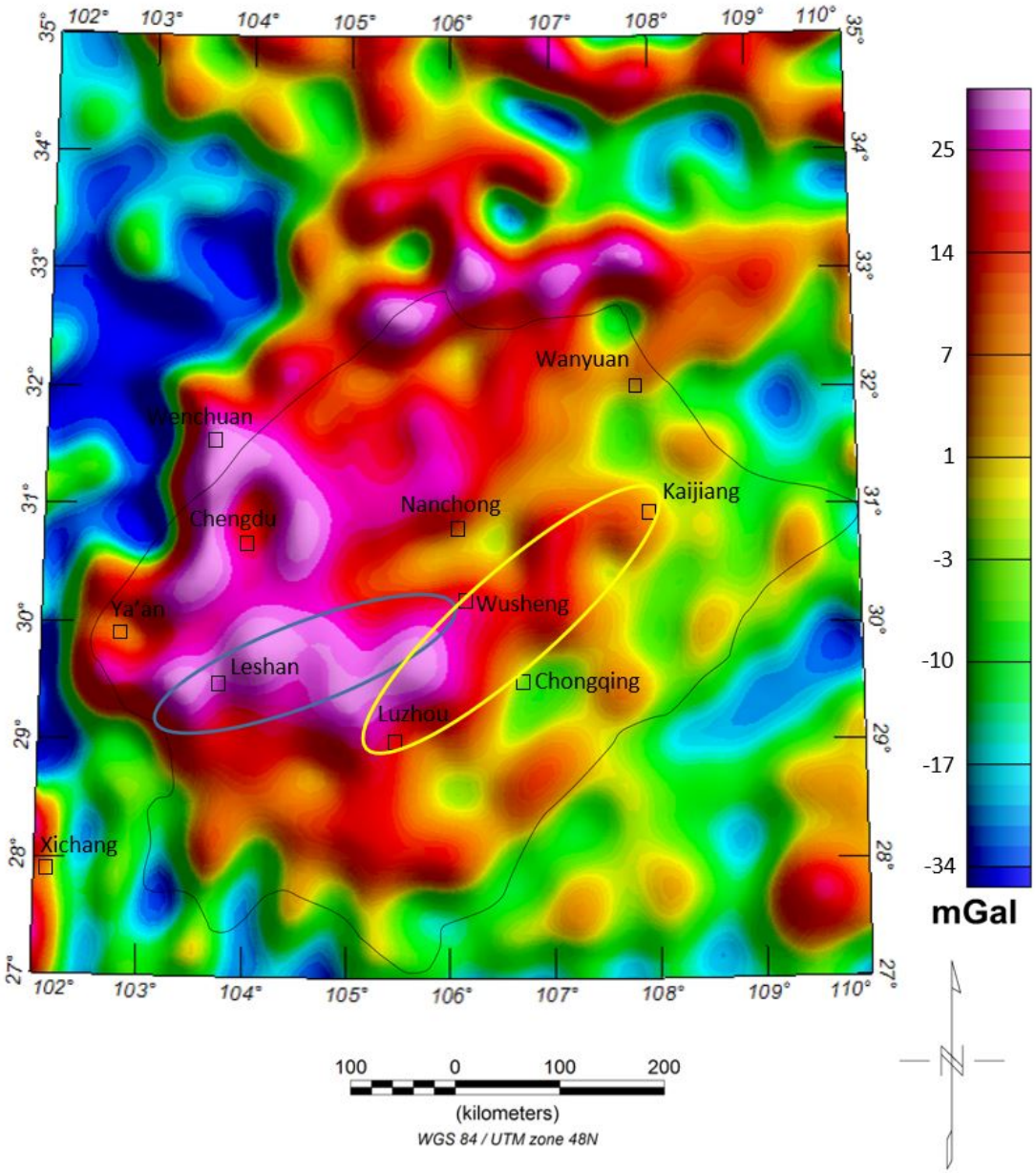

Figure 4.9. Residual gravity anomaly map of the Sichuan Basin, by subtracting the 10 km upward continued grid from the CBA grid. Comparing with 40 km upward filter, the shallower gravity anomalies are migrating to the east, implying the central paleo-uplift is also moving east. The map symbols are the same as Figure 4.8.

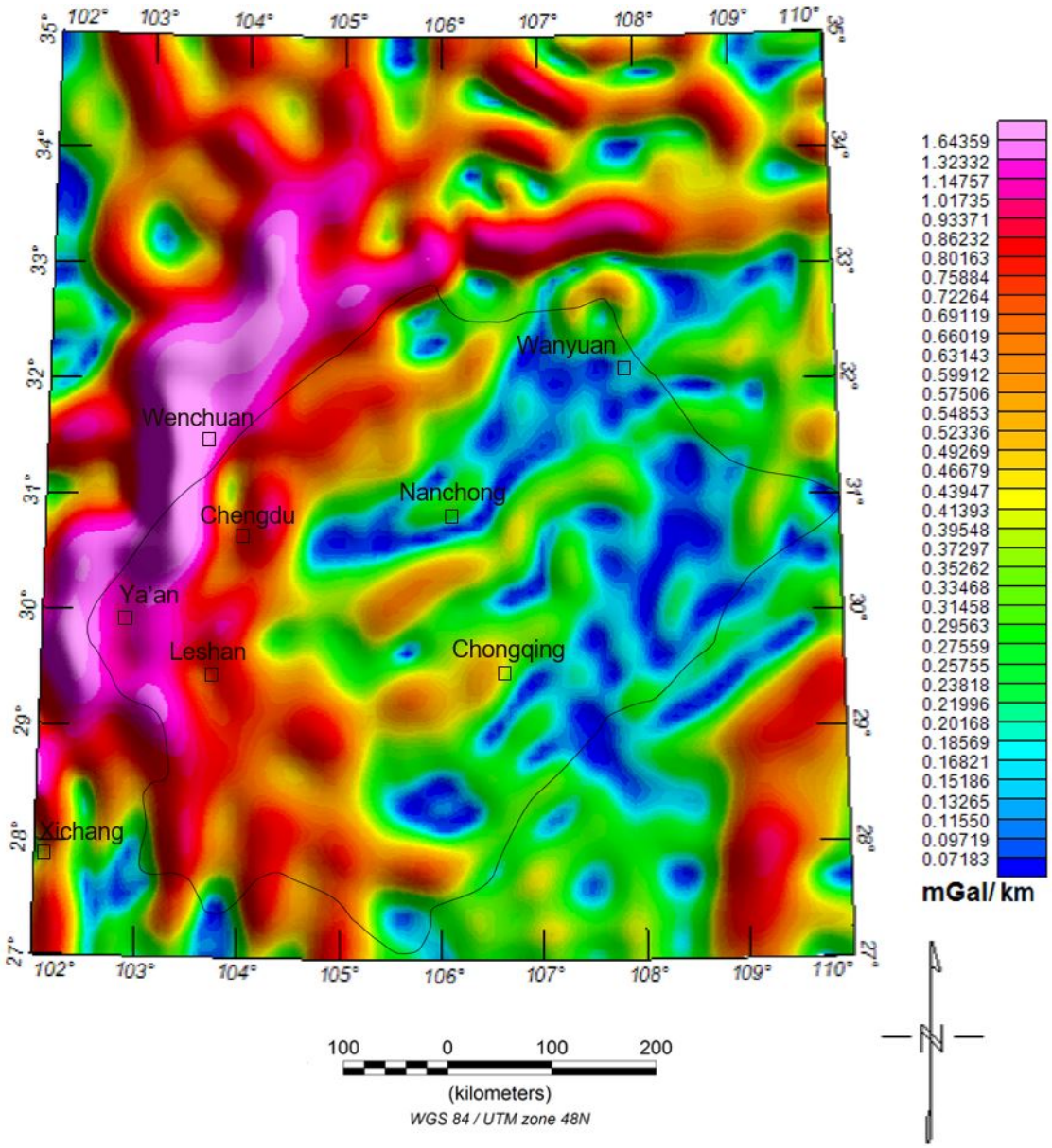

Figure 4.10. Horizontal gradient magnitude (HGM) of the CBA of the Sichuan Bain. HGM filter can effectively recognize and emphasize the structural details of study area, such as edges and trends of subsurface geologic bodies. The map symbols are the same as Figure 4.1.

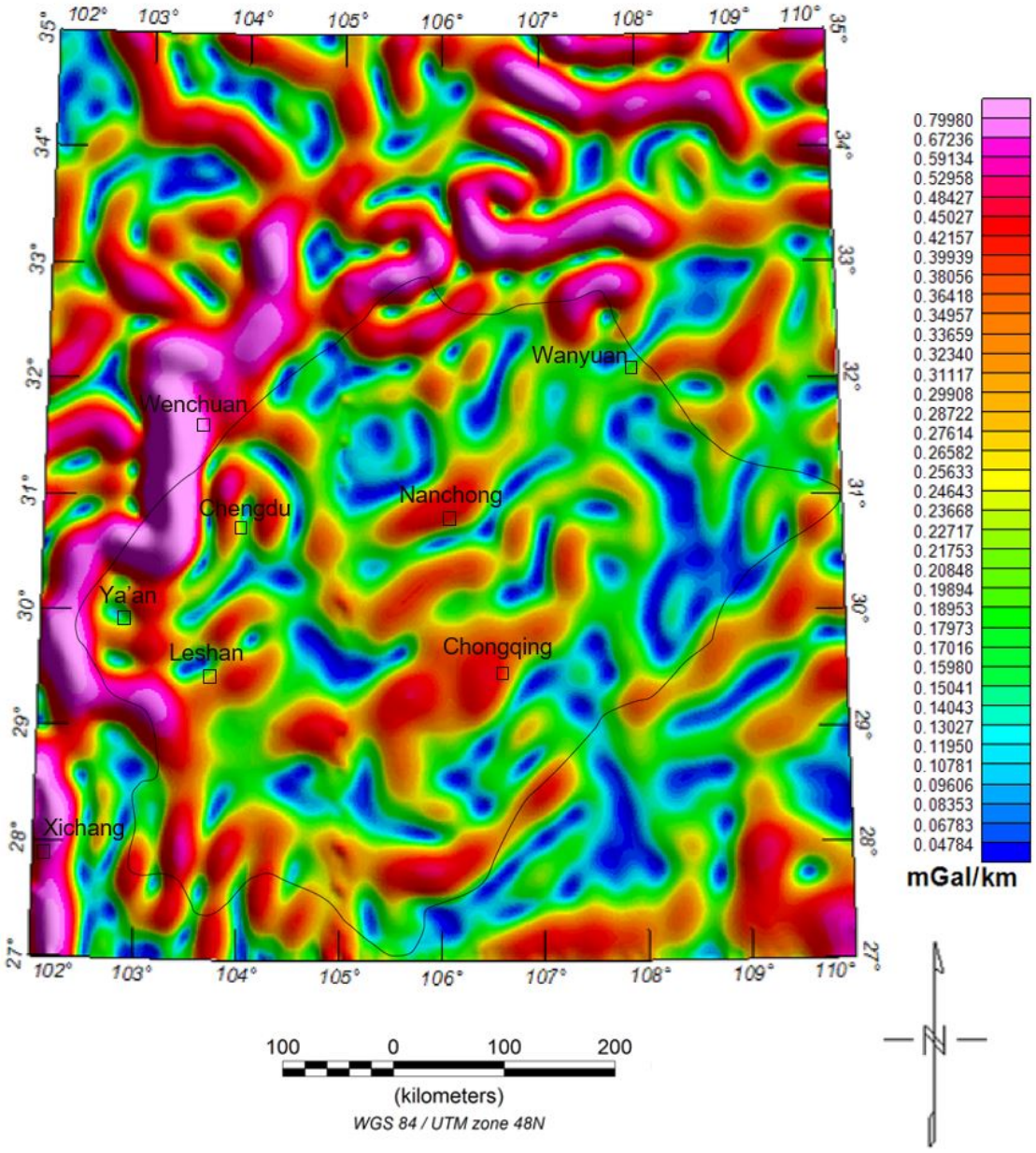

Figure 4.11. Horizontal gradient magnitude (HGM) of the residual gravity after 40 km upward continuation of the Sichuan Bain. The map symbols are the same as Figure 4.1.

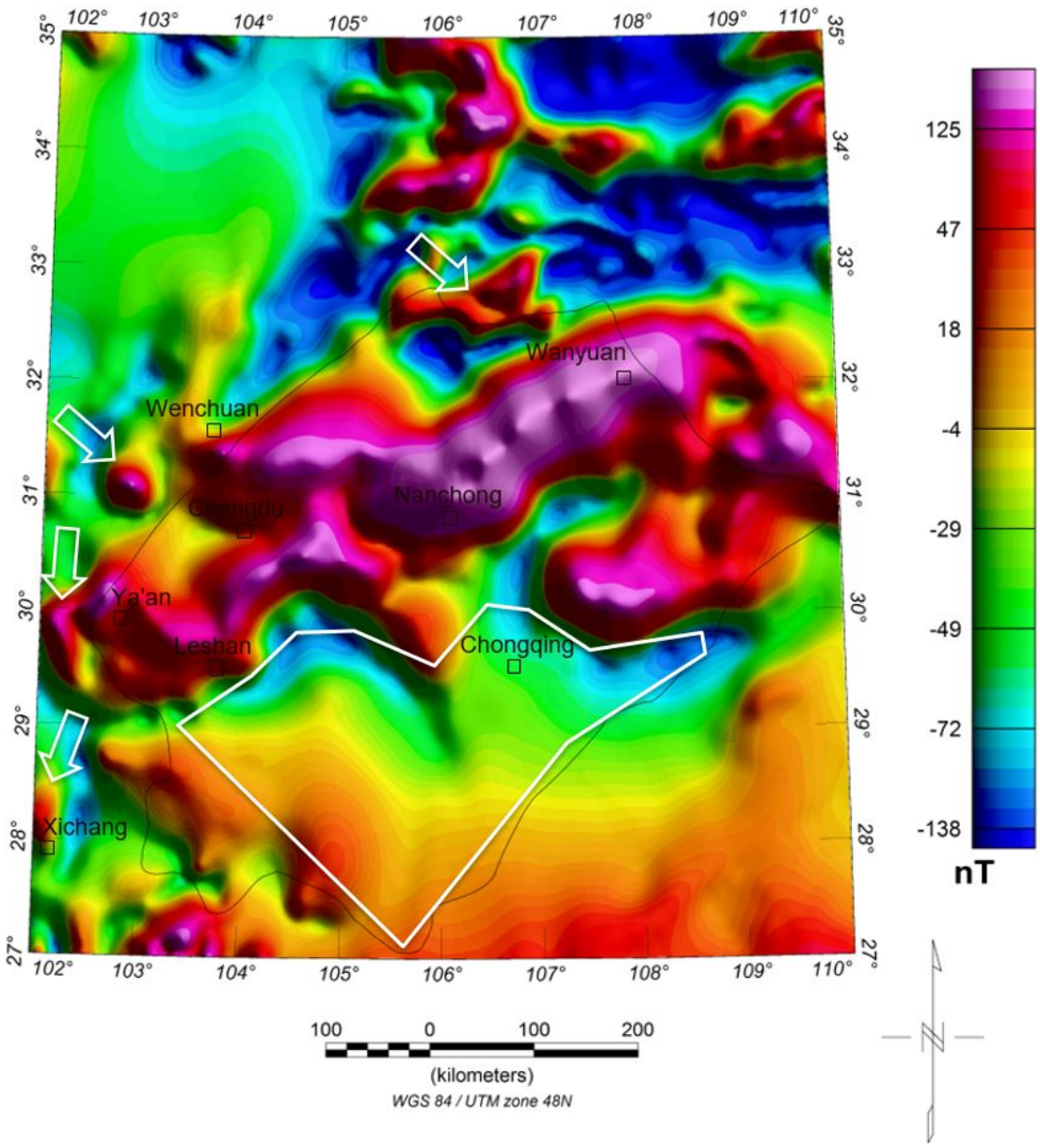

Figure 4.12. Total magnetic intensity (TMI) after reduced to pole (RTP) of the Sichuan Bain. All magnetic data courtesy of WDMAM project. Note that magnetic highs concentrate along Nanchong – Wanyuan. Besides, Micangshan, Wenchuan, Ya'an, and Xichang are characterized as scattered magnetic highs (see white arrows). Southeastern half of the basin is outlined in white. The map symbols are the same as Figure 4.1.

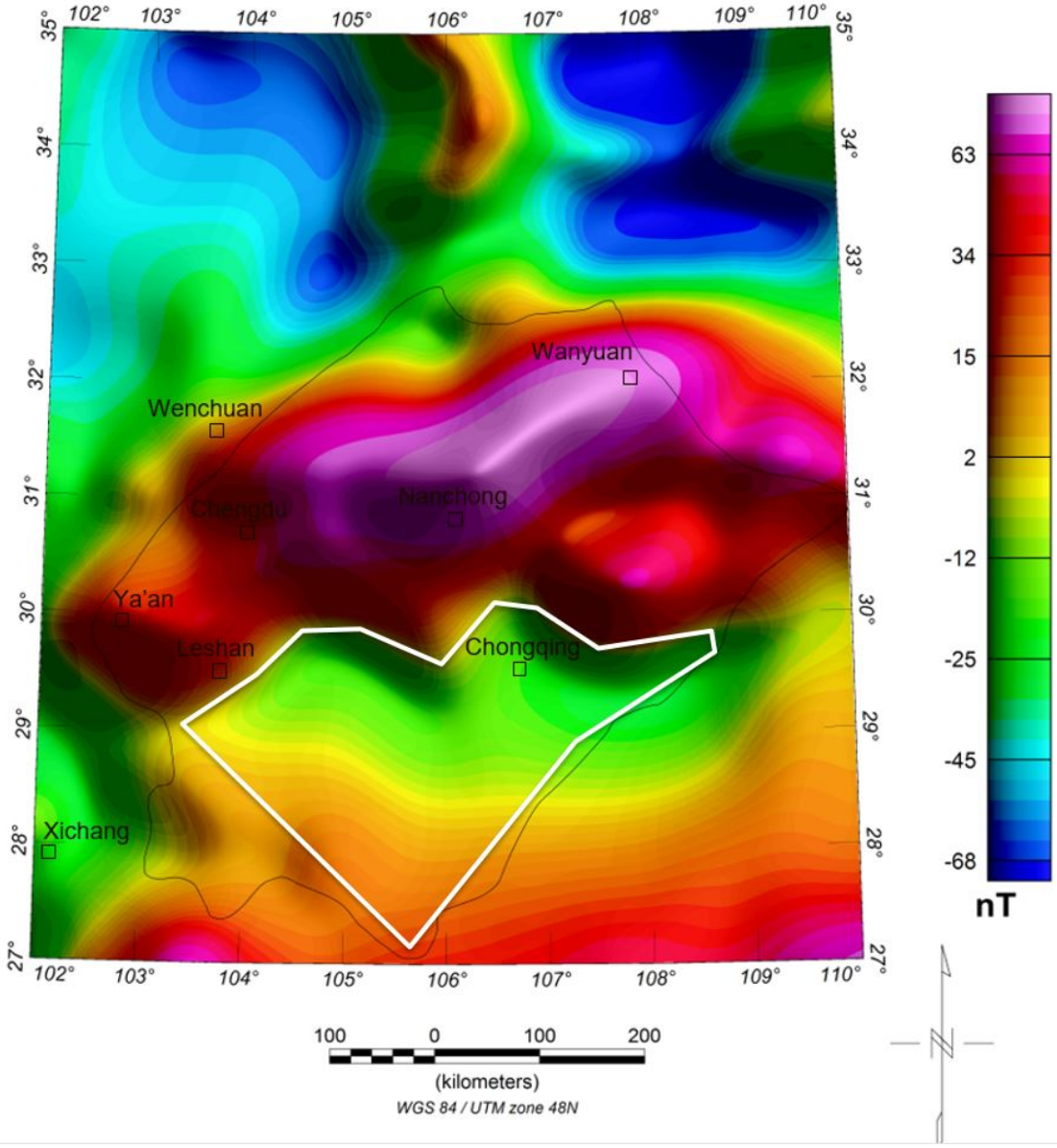

Figure 4.13. Total magnetic intensity (TMI) after 40 km upward continuation of the Sichuan Bain. Note that the deep magnetic anomalies still follow Nanchong-Wanyuan, which suggests that the magnetic body was buried in a deep depth. In addition, scattered magnetic highs recede, such as Xichang, Wenchuan. It implies these local high anomalies were cause by shallow magnetic body intrusions. The map symbols are the same as Figure 4.1.

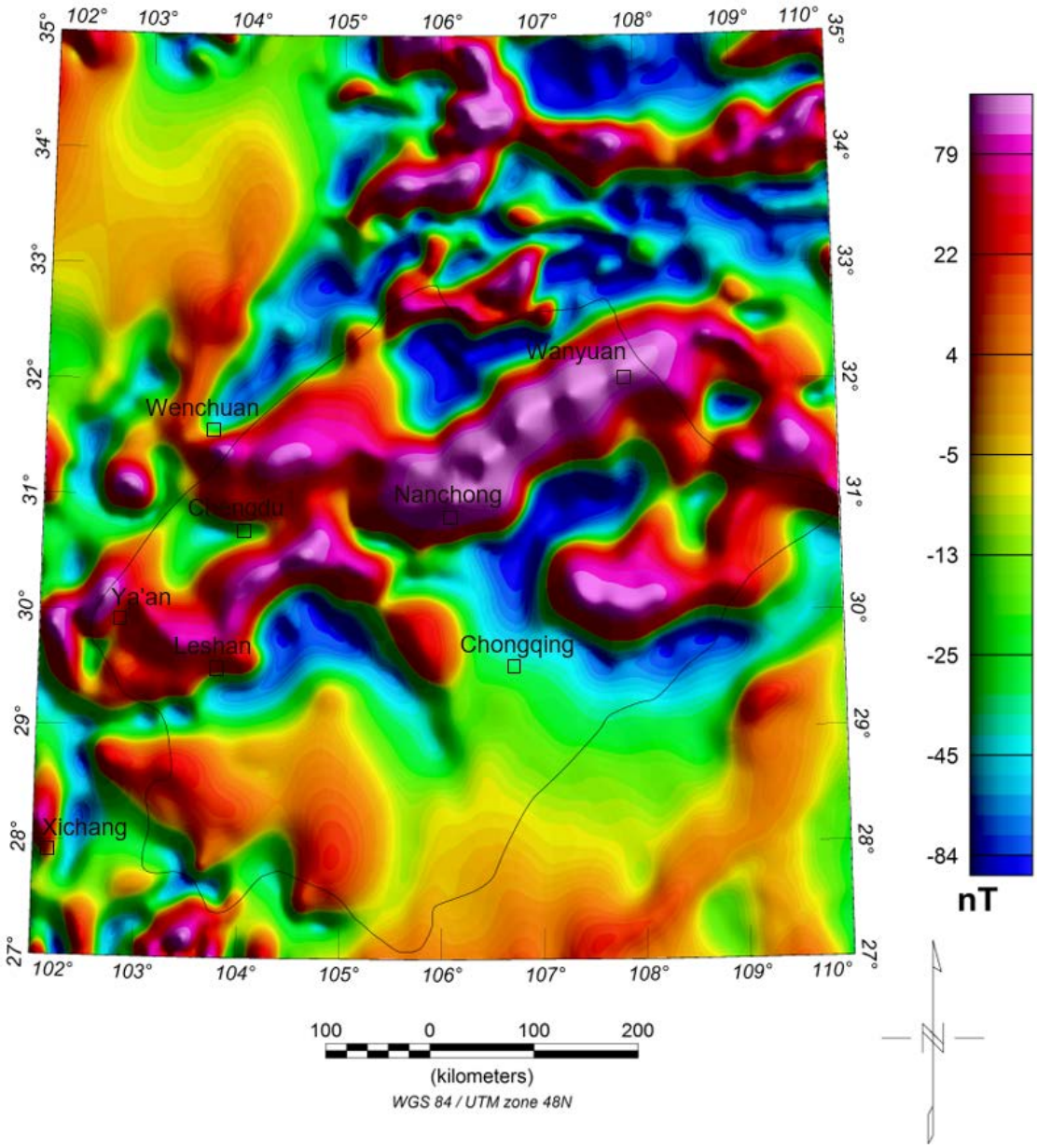

Figure 4.14. Residual magnetic map of the Sichuan Basin, by subtracting the 40 km upward continued grid from the RTP grid. Comparing Figures 4.12 and 4.14, the residual magnetic map is highly consistent with the original RTP map, which clearly documents that in the study area, the magnetic anomalies are dominated by shallow crustal features. The map symbols are the same as Figure 4.1.

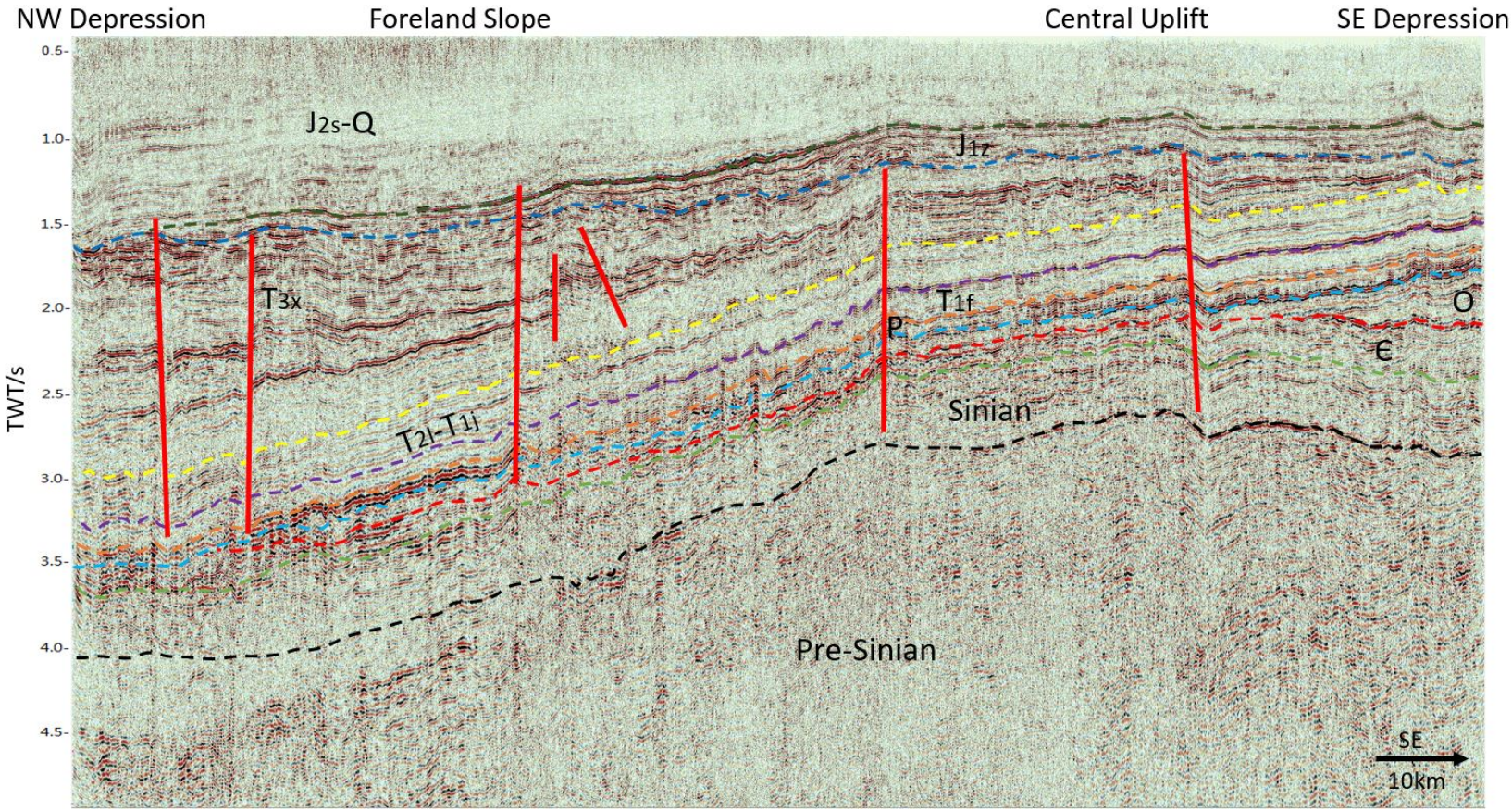

Figure 4.15. Interpretation of Section A (See location in Figure 3.2). Well-developed normal faults in NW Depression are mapped in red lines. Q-Quaternary, J_{2s}-Shaximiao Formation (Middle Jurassic), J_{1z}-Ziliujing Formation (Lower Jurassic), T_{3x}-Xujiahe Formation (Upper Triassic), T_{2l}-Leikoupo Formation (Middle Triassic), T_{1j}-Jialingjiang Formation (Lower Triassic), T_{1f}-Feixianguan Formation (Lower Triassic), P-Permian, O-Ordovician, ∈-Cambrian (See generalized stratigraphy column in Figure 2.3)

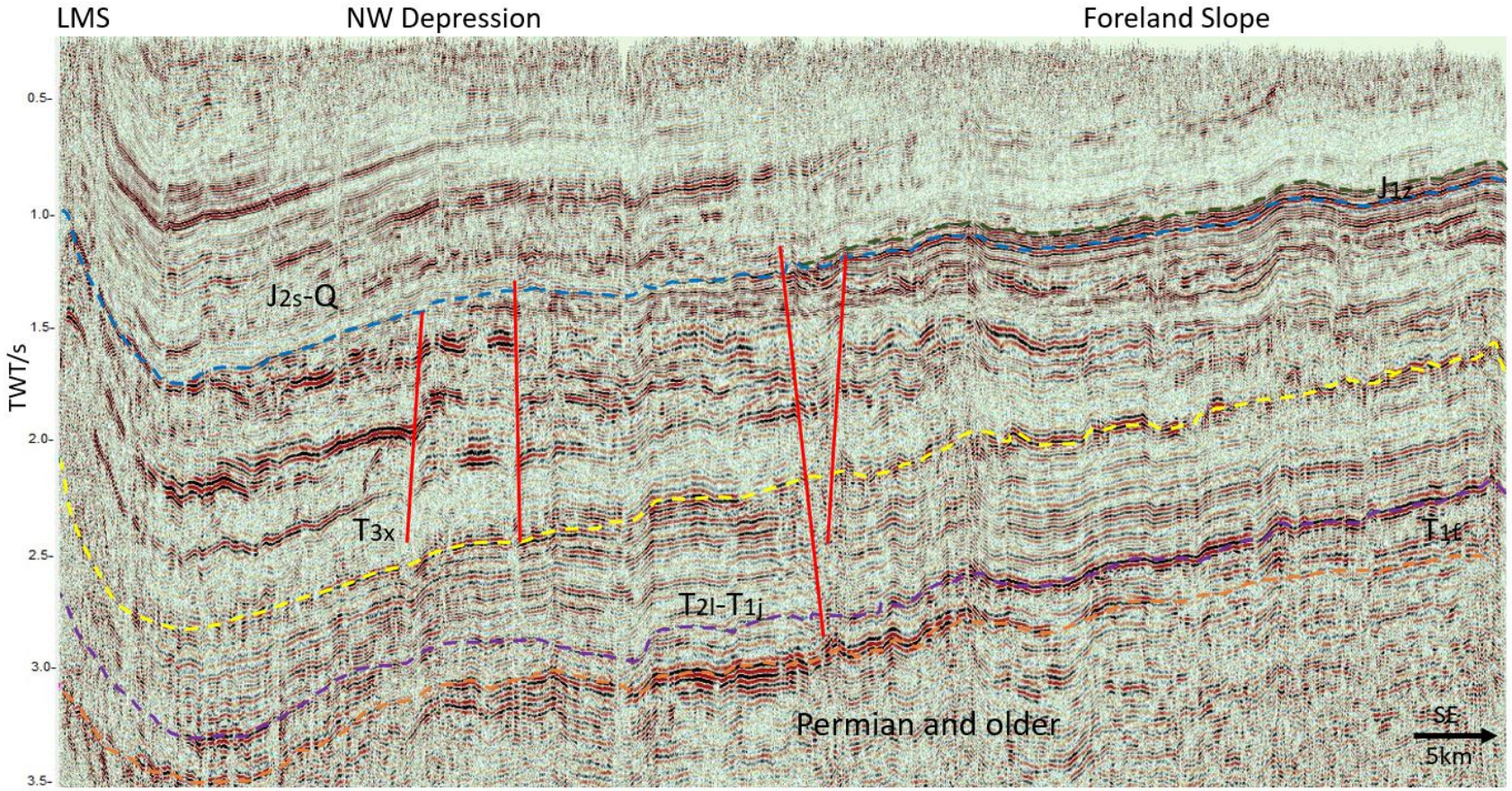

Figure 4.16. Interpretation of Section B (See location in Figure 3.2). Normal faults are mapped in red lines. LMS-Longmenshan, Q-Quaternary, J_{2s}-Shaximiao Formation (Middle Jurassic), J_{1z}-Ziliujing Formation (Lower Jurassic), T_{3x}-Xujiahe Formation (Upper Triassic), T_{2l}-Leikoupo Formation (Middle Triassic), T_{1j}-Jialingjiang Formation (Lower Triassic), T_{1f}-Feixianguan Formation (Lower Triassic) (See generalized stratigraphy column in Figure 2.3).

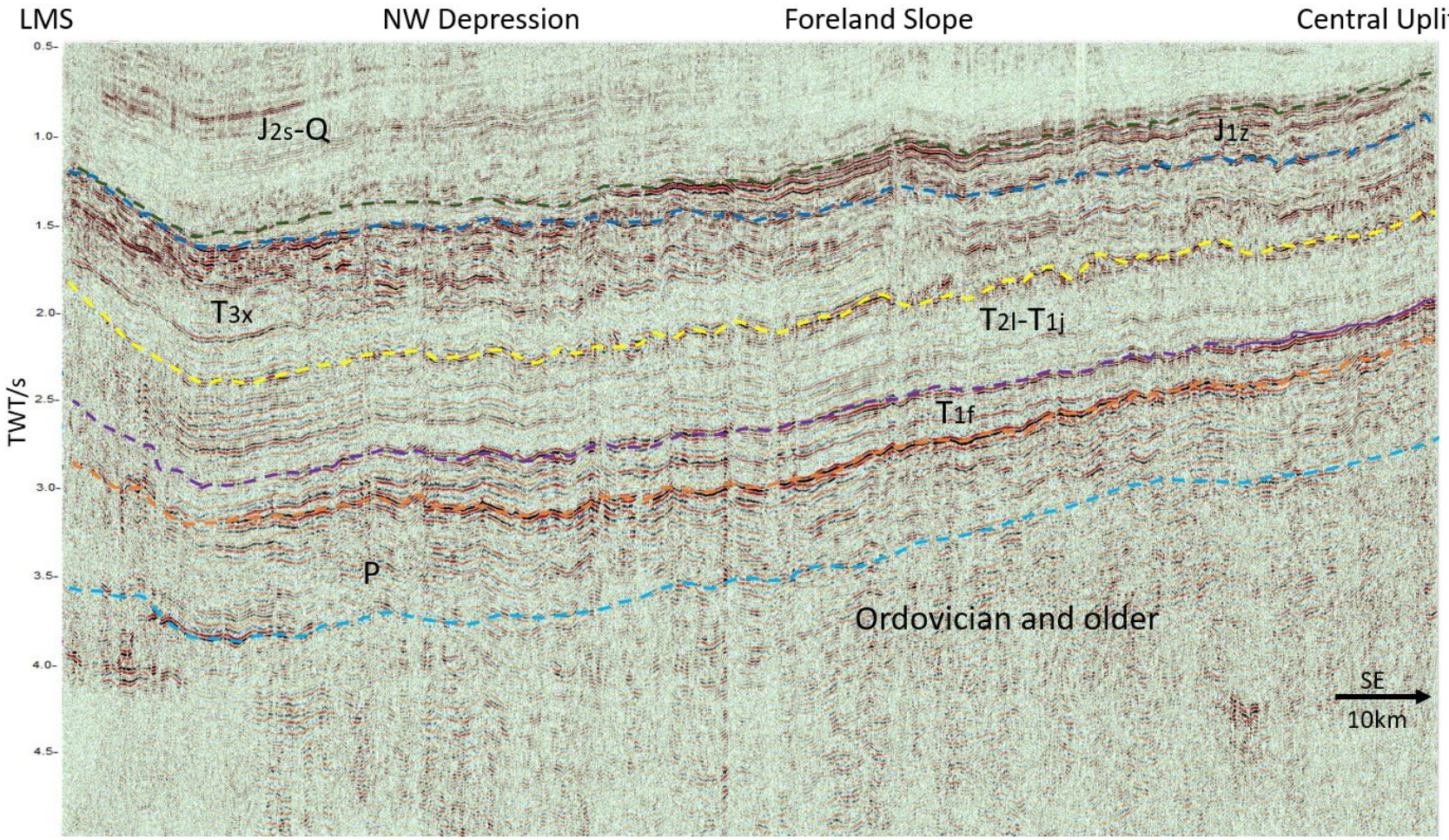

Figure 4.17. Interpretation of Section C (See location in Figure 3.2). LMS-Longmenshan, Q-Quaternary, J_{2s}-Shaximiao Formation (Middle Jurassic), J_{1z}-Ziliujing Formation (Lower Jurassic), T_{3x}-Xujiahe Formation (Upper Triassic), T_{2l}-Leikoupo Formation (Middle Triassic), T_{1j}-Jialingjiang Formation (Lower Triassic), T_{1f}-Feixianguan Formation (Lower Triassic), P-Permian (See generalized stratigraphy column in Figure 2.3).

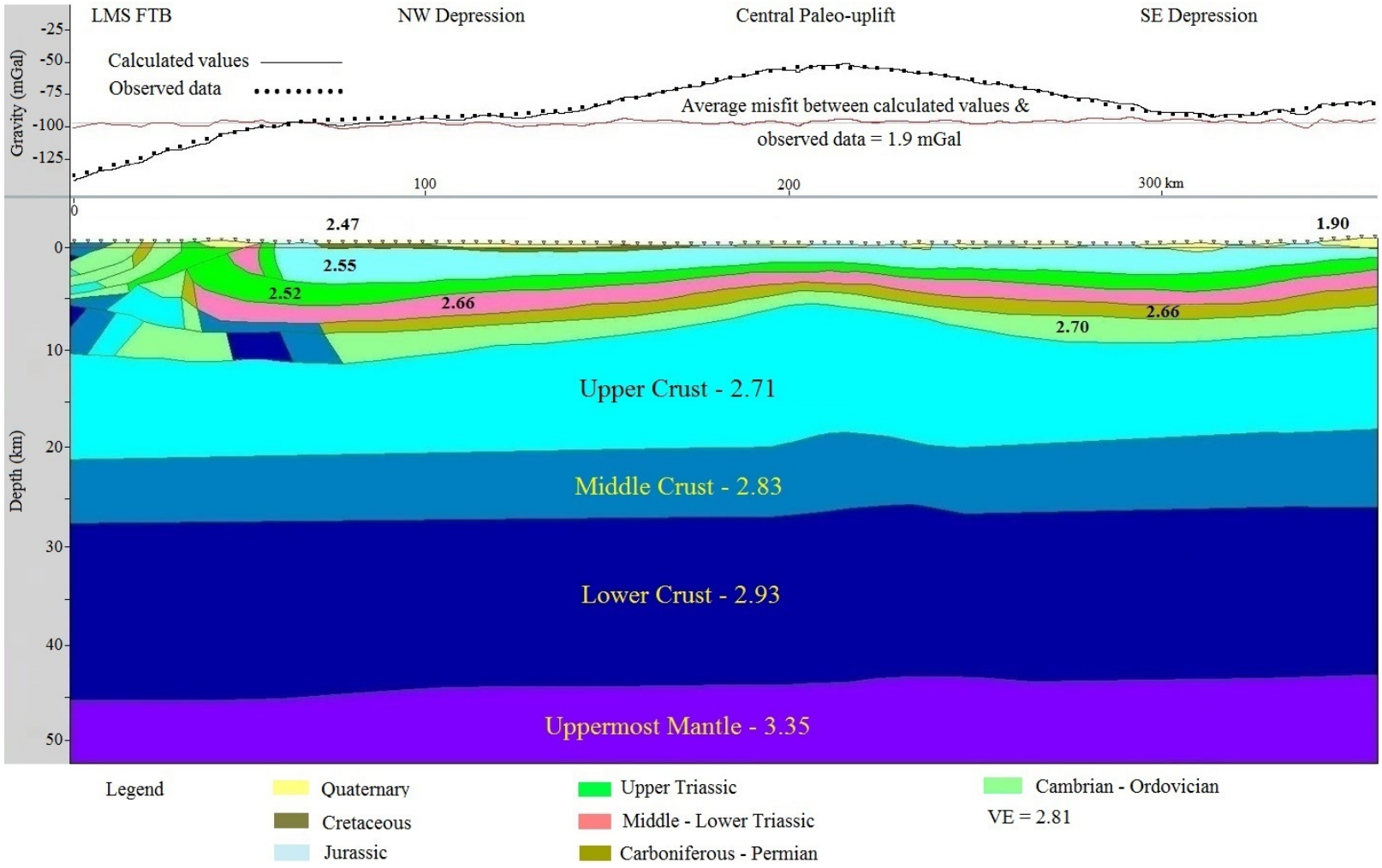

Figure 4.18. Integrated 2-D gravity model of Section D (See location in Figure 3.2). VE is vertical exaggeration. The values on the model are density values in g/cm^3 (See Table 4.1). LMS FTB-Longmenshan fold-thrust belt.

Gas Field Name	Proved Reserves (10^8 m^3)	Gas Bearing Layers	Reservoir Rock Types
Puguang	4050.79	T, P	Carbonates
Guangan	1355.58	T3x	Clastics
Hechuan	1187.06	T3x	Clastics
Datianchi	1067.55	T, P, C	Carbonates
Xinchang	843.02	T, J	Clastics
Luojiazhai	797.36	T, P, C	Carbonates
Moxi	702.31	T	Carbonates
Wolonghe	408.61	T, P	Carbonates
Weiyuan	408.61	P, Z	Carbonates
Tieshanpo	373.97	T	Carbonates
Dukouhe	359	T	Carbonates
Bajiaochang	351.07	J, T	Clastics
Luodai	323.83	J	Clastics
Qiongxi	323.25	J, T	Clastics

Table 3.1 Features of the large size gas fields in Sichuan Basin. Modified from Ma et al., 2010. (See gas fields location in Figure 3.1)

Stratum	Density (10^3kg/m^3)
Quaternary	1.9
Paleogene-Neogene	2.18
Cretaceous	2.47
Jurassic	2.55
Upper Triassic	2.52
Middle Triassic	2.66
Lower Triassic	2.66
Carboniferous-Permian	2.66
Silurian-Devonian	2.68
Cambrian-Ordovician	2.7
Upper Crust	2.71
Middle Crust	2.83
Lower Crust	2.93
Uppermost Mantle	3.35

Table 4.1 Density of different stratum in the Sichuan Basin. Modified from Lin and Zhu, 1993; Liu and Chang, 2003; Zhang., 2010; Jiang et al., 2012.